Cement and Concrete Composites 132 (2022) 104643

Contents lists available at ScienceDirect

Cement and Concrete Composites

journal homepage: www.elsevier.com/locate/cemconcomp

A lignin-based capsule system with tunable properties tailored for robust self-healing concrete

Arkabrata Sinha, Darren Zhen Hui Lim, Jianqiang Wei *

Department of Civil and Environmental Engineering, Francis College of Engineering, University of Massachusetts Lowell, Lowell, MA, 01854, USA

ARTICLE INFO

Keywords:
Self-healing concrete
Biomass capsules
Lignin
Compatibility
Cracks
Property recovery

ABSTRACT

Self-healing is an ideal mechanism for concrete to achieve self-repair of microcracks. While extensive efforts have been invested in capsule-based autonomous self-healing, the dilemma between capsules' survivability during concrete mixing and their rapture upon concrete cracking to release healing agents remains unsolved. This study aims to address this challenge by investigating a lignin-based capsule system with tunable properties in concrete. Ellipsoidal capsules with varying dimensions, aspect ratios and shell thicknesses manufactured via 3D printing are investigated in terms of survivability, degradation kinetics, mechanical compatibility, self-healing capacity, concrete property recovery and microstructure analyses. The results indicate exceptional survivability of the capsules with intact and survival ratios of 100% and 95%, respectively. By leveraging the alkaline degradation and mineralization of lignin, tunable capsule properties are triggered with 88.5% strength and 57.3% rapture strain decreases after 3 h in pore solution and a 57.6% degradation degree in concrete after 28 days, which ensure robust release of healing agents. No negative impact on first cracking strength was observed by embedding capsules over the predicted crack path, and the 120-h crack width and cracking density are reduced by 64.3% and 84%, respectively. After 14 days, 78.7% of first cracking strength and 94.5% of bulk resistance are recovered.

1. Introduction

Concrete, the most consumed material only after water, is inherently quasi-brittle in nature, which makes it susceptible to cracking. Concrete cracking commonly occurs under environmental or mechanical loadings in terms of weathering, shrinkage, creep, chemical attacks, subgrade settlement, and thermal stress. Mechanically, the presence of cracks reduces the effective cross-sectional area, flexural rigidity, shear modulus, and fracture toughness of concrete structures. More importantly, the formation of cracks can provide new transport paths for heat, moisture, and external chemical reactants into concrete thereby leading to a variety of deterioration issues such as corrosion of steel reinforcement [1,2], alkali-silica reaction [3,4], sulfate attack [5], carbonation [6], and freeze-thaw damage [7]. A direct result of these fatal deteriorations is the decreased long-term durability or even premature failure of structures. This remains an intractable problem that shortens the lifetime of concrete structures and costs billions of dollars for maintenance each year [8,9], which is 84% to 126% higher than the cost of the material itself [10,11]. According to a version 2020 for concrete repair protection published in 2004 [8], in the United States alone, $18–21 billion was estimated as the annual economic impact associated with maintaining, rehabilitating or strengthening aged concrete structures. This demonstrates that the annual cost is between $2.00 and $2.33 per cubic yard of in-place concrete (with an assumption of 60% of the 15 billion cubic yards placed since 1930 is still in place) [8]. Associating with the increased maintenance costs is the increasingly negative environmental impact of cement manufacturing and consumption. In the past 90 years, the global cement production has been increased by 5777% and the cement-related annual CO_2 emissions have been raised to 2.5 Gt [12–14], approximately 8% of the global CO_2 emissions [15]. Given its ubiquity, an extension of the service life of concrete structures would result in less cement consumption thereby a significant influence on sustainability and climate change.

Outperforming the traditional repair techniques, such as epoxy injection [16–18], electrodeposition [19,20], and grouting [21,22] that involve complicated machinery and significant manpower and are only able to heal surface cracks up to a limited depth, self-healing has been proven a promising approach to reduce maintenance costs as cracks can

* Corresponding author. Department of Civil and Environmental Engineering, University of Massachusetts Lowell, 1 University Avenue, Shah Hall 200, Lowell, MA, 01854, United States.
E-mail address: Jianqiang_wei@uml.edu (J. Wei).

https://doi.org/10.1016/j.cemconcomp.2022.104643
Received 26 February 2022; Received in revised form 13 June 2022; Accepted 19 June 2022
Available online 23 June 2022

be autonomously repaired inside-out without human intervention [23]. As summarized in Table 1, to date, two self-healing approaches have been employed for concrete. By leveraging the continuous hydration of anhydrous cement particles [24,25] or in-situ carbonation of cement hydrates [24,26] in the crack zones, intrinsic (autogenous) self-healing is an ideal concept for concrete. However, this intrinsic self-healing approach depends heavily on the age of concrete, in which the hydration of unhydrated cement and the carbonation of hydrated products get less robust in old concrete over time. Moreover, the supply of water is indispensable to trigger the hydration and carbonation reactions. As a result, the self-healing efficiency is limited, and only narrower cracks with a width less than 300 μm can be healed [24–31]. Different from autogenous self-healing, autonomous self-healing approaches are achieved via the incorporations of external agents, such as mineral admixtures [32], supplementary cementitious materials [33], polymers [34–39], sodium silicate solutions [40–42], bacteria [43–47] and fungi [48–51]. Table 1 summarizes the current state of intrinsic and autonomous approaches with a variety of mechanisms and triggers for self-healing concrete. Regardless of the mechanisms and triggers, autonomous self-healing approaches exhibit efficient crack repairing performance outperforming intrinsic self-healing mechanisms, while the self-healing agents need to survive during the harsh concrete mixing and keep dormant in the alkaline hydrated cement matrix until to be activated upon concrete cracking. Therefore, capsules play critical roles in preventing the core healing agents and determining the crack healing efficiency.

To date, a variety of capsule shell materials have been investigated for carrying healing agents in self-healing systems including urea-formaldehyde [59–62], polylactic acid (PLA) [42], glass [63–68], expansive clays [69,70], plant fibers [71,72], ceramic [73], perspex [66], wax [74], silica and silica gel [75–77], paraffin [78,79], diatomaceous earth [80], porous concrete [81] low alkali cementitious materials [82], polymethyl methacrylate [61,62], low alkali cementitious materials [82], recycled brick aggregates [83], sugar-coated expanded perlite [84] and carbide slag fly ash and desulfurized gypsum [85]. While extensive research efforts have been conducted in this field, the self-healing efficiency and robustness of the studied systems are still less than anticipated. A primary reason lies in the critical challenge that remains unsolved for years: the dilemma between the capsules' resistance again concrete mixing (survivability) and the efficient rupture to release healing agents upon concrete cracking (easy damage), which are mechanically opposite to each other.

Table 1
Self-healing approaches for concrete.

Category	Mechanism	Trigger	Need of encapsulation	Reference
Intrinsic	Hydration of unhydrated cement	Moisture	No	[24,25]
	Carbonation of hydrated cement	CO_2 and moisture	No	[24,26]
Autonomous	Cementing action and crystal formation of mineral admixtures	Water	Yes	[52]
	Formation of C–S–H[a] and calcite with additions of SCMs[b]	Water	No	[33]
	Polymerization of encapsulated monomer and catalyst	Catalyst chemicals	Yes	[53]
	Formation of C–S–H from silicates	Moisture	Yes	[40–42]
	Calcite precipitation by bacteria via ureolysis, nitrate reduction and aerobic oxidation	Nutrients, CO_2, calcium or nitrate	Yes	[43,44, 46,54]
	Calcite precipitation by Fungi	Nutrients, CO_2, or calcium	Yes	[48–51]
	Air curing of Cyanoacrylates	Air or moisture	Yes	[55,56]
	Heat or air curing of epoxy	Air or moisture	Yes	[57,58]

[a] C–S–H: calcium silicate hydrates.
[b] SCM: supplementary cementitious materials.

To address the aforementioned difficulties and challenges, a novel capsule system with both high survivability and effective healing agent release is desired. Towards this end, a sustainable biomass capsule-based self-healing system derived from lignin is investigated in this study. Lignin, the second most abundantly available biopolymer in the world after cellulose, is a byproduct of the pulp and paper-making industry [86]. In addition to being cost-effective over synthetic polymers, such as acrylonitrile butadiene styrene (ABS), Polyethylene terephthalate (PET), Polyether ether ketone (PEEK), polypropylene (PP), and nylon, lignin is environmentally more sustainable, renewable and biodegradable and obtainable from various plants [87]. In addition to these merits, the unique alkaline degradation behavior of this biopolymer can be leveraged to trigger a switchable property of the capsules, namely high survivability to survive the concrete mixing process and degradable strength to guarantee easy rupture in the presence of concrete cracking. With this anticipation, a comprehensive investigation on a lignin-based capsule system synthesized via precise 3D printing is conducted in the present study. The ability of lignin capsules with a variety of dimensional and geometrical characteristics to withstand concrete mixing was evaluated. The property tunability was dually verified via micro-tensile tests on dog-bone specimens conditioned in a simulated concrete pore solution and thermogravimetric analysis (TGA) on the capsules extracted from concrete. The compatibility of the lignin capsules with concrete was elucidated based on the evolutions of concrete mechanical properties and the microstructure of interfacial bond between the capsules and the cement matrix. The self-healing capability of the concrete containing the lignin capsule system filled with sodium silicate solution as a self-healing agent was evaluated by monitoring the post-cracking strength and permeability recovery and crack closure behavior.

2. Materials and methodology

2.1. Materials

A lignin-based filament with a diameter of 1.75 mm, density of 1.23 gm/cm^3 and Vicat softening temperature of 48 °C was used to manufacture the capsules in this study. The tensile strength, flexural strength, and flexural modulus of the filament are 40 MPa, 43 MPa, and 3,200 MPa, respectively. A TGA test of the filament showed that the onset and burnout degradation temperature occurred in two steps between 250-375 °C and 275–450 °C. A reagent-grade sodium silicate (Na_2SiO_3) solution containing 10.6% NaO_2 and 26.5% SiO_2 by mass, respectively, was used as the healing agent. Type I/II Ordinary Portland cement, all-purpose sand, and 3/8-inch gravels were used for concrete specimens. Table 2 summarized the chemical and mineral compositions of the cement. The specific gravity of the cement, fine and coarse aggregate were 3.15, 2.7, and 2.6, respectively. Sufficient workability and low segregation of concrete were ensured by mixing a high-efficiency poly carboxylate-based superplasticizer (ADVA® Cast 555). A simulated pore solution with a pH value of 13.47 was prepared using reagent-grade sodium hydroxide with a purity of over 97.0%, calcium hydroxide with a purity of over 99%, potassium hydroxide with a purity of over 85%, potassium sulfate, sodium metasilicate, sodium aluminate and deionized water. The composition summarized in Table 3 was employed to simulate the real pore solution from cement at 70 days according to

Table 2
Chemical and mineralogical compositions of Type I/II Portland cement.

Chemical composition (%)	SiO_2	Al_2O_3	Fe_2O_3	CaO	MgO	SO_2	CO_2
	19.9	4.8	3.1	62.2	3.4	3.6	0.5
Mineral components (%)	C_3S[a]	C_2S[b]	C_3A[c]	C_4AF[d]	LS[e]	Equivalent alkalis	
	53	17	7	9	1.2	0.60	

[a] C_3S: tricalcium silicate.
[b] C_2S: dicalcium silicate.
[c] C_3A: tricalcium aluminate.
[d] C_4AF: tetra-calcium aluminoferrite.
[e] LS: limestone.

Table 3
Composition of simulated pore solution.

Chemical	$Ca(OH)_2$	Na_2SiO_3	$NaAlO_2$	KOH	K_2SO_4	NaOH
Mass (gm/L)	0.1111	0.0256	0.0090	29.4852	9.9737	2.5786

Ref. [88]. Brass-coated steel microfibers with a diameter of 0.2 mm, length of 12.95 mm, and average tensile strength of 2,903 MPa were used as reinforcement for mortar beams.

2.2. Sample preparation

Spherical and elliptical lignin capsules with varying dimensions and shell thickness were manufactured via fused deposition modeling (FDM) 3D printing using an Anycubic 4Max Pro printer with a 0.4 mm nozzle head. An extruder temperature of 175 °C, a bed temperature of 60 °C, a printing speed of 60 mm/s and a layer thickness of 0.1 mm were employed for high print quality and to avoid printing defects. To investigate the effect of geometry and size on the survivability of the capsules against the harsh concrete mixing, capsules with minor diameters between 9.5 mm and 19.5 mm in accordance with the nominal size of gravel used in concrete were manufactured. As summarized in Table 4, the aspect ratios varying from 1 to 2 and shell thicknesses varying from 0.4 mm to 2.0 mm were employed. Selected capsule groups are shown in Fig. 1. To uncover the influence of sand-level capsules on the mechanical properties of mortar, smaller capsules with a minor diameter of 5 mm, an aspect ratio of 1.5 and shell thickness of 0.2 mm were also prepared. The capsules were injected with the healing agent sodium silicate solution and sealed with the same filament material with a hot needle to study the self-healing efficacy of the system. Dogbone specimens with a gauge length of 7.5 mm, gage width of 2 mm and gauge thickness of 0.4 mm were prepared via the same 3D printing method for a micro-tensile test to investigate the degradation behavior of the capsule material in the alkaline cement pore solution. After multiple iterations, the print speed and layer thickness were set at 60 mm/s and 0.06 mm, respectively, to obtain the optimum print quality.

Table 4
Geometric specifications for lignin capsules.

Group		Minor diameter (mm)	Major diameter (mm)	Aspect ratio	Shell thickness (mm)
Sand level	S1	5	7.5	1.5	0.2
Gravel level	G1	19.05	19.05	1	0.8
	G2	19.05	28.575	1.5	0.8
	G3	12.7	19.05	1.5	0.8
	G4	19.05	38.1	2	0.8
	G5	9.5	9.5	1	0.4
	G6	9.5	19.05	2	0.4
	G7	9.5	19.05	2	0.8
	G8	9.5	14.25	1.5	0.4
	G9	9.5	14.25	1.5	0.8
	G10	9.5	14.25	1.5	1.2
	G11	9.5	14.25	1.5	1.6
	G12	9.5	14.25	1.5	2

Cylindrical concrete specimens with a diameter of 75 mm and height of 150 mm were cast using cement, sand, and gravel in a ratio of 1:2:3 with a water to cement ratio of 0.4. The ADVA® Cast 555 superplasticizer was used at a dosage of 0.014 ml per 100 g of cement, to maintain workability and prevent segregation. The moisture absorption capability of the aggregates was considered to adjust the amount of mixing water. Previous studies have shown that the optimum volume fraction of capsules to achieve sufficient self-healing without affecting the mechanical properties of concrete varied between 2% and 5% [89]. In this study, a volume fraction of 5% was employed to assess the compatibility of the lignin-based capsules in the concrete matrix and their effect on mechanical strength. The concrete was mixed using a Gilson Brothers Co. concrete mixer following ASTM C192 [90]. After obtaining a homogeneously mixed concrete matrix, the capsules were added followed by an additional 5 min of mixing to ensure uniform distribution of the capsules. The slump test carried out according to ASTM C143 [91] showed that the slump of fresh concrete increased from 38 mm to 119 mm in the presence of lignin capsules indicating improved workability.

Cubic 50 mm by 50 mm by 50 mm mortar specimens containing the sand-level lignin capsules at a volume fraction of 2% were prepared to evaluate the compatibility and influence on mechanical strength. The same cement and sand as those in concrete at a water to cement ratio of 0.4 and a cement to sand ratio of 1:2 were used. with the same proportions, mortar cylinders with a diameter of 75 mm and height of 150 mm containing the gravel-level capsules at a volume fraction of 3.5% were prepared to monitor the bulk resistivity due to the self-healing of cracked specimens. Two 40 mm by 75 mm by 254 mm mortar beams with a 6.5 mm deep and 3.15 mm wide notch at the midspan were prepared for crack-healing efficacy and property recovery evaluations. Three gravel-sized capsules (G8) filled with sodium silicate solution with equal intervals were placed at a depth of 20 mm (13.5 mm right above the notch), which yields a distance of 15.25 mm between the beam top surface and the capsule top. One beam without capsules was prepared for comparison. The mortar for the beams had the same mix design as the cubes with an addition of 2% volume fraction of steel fibers to improve ductility and the ease of micro-crack creation. All the concrete cylinders, mortar cubes and beams were demolded after 24 h of casting followed by curing in saturated lime solution at room temperature (23 ± 2 °C) until testing.

To investigate the degradation behavior of lignin capsules in the concrete environment at an elevated temperature, 50 mm by 50 mm by 50 mm mortar cubes at a water-cement ratio of 0.4 with 2 gravel-level capsules embedded in the center were cast. After demolding, the cubic samples were cured in saturated lime solution at 50 °C until testing.

2.3. Experimental procedures

2.3.1. Survivability test

The survivability and functionality of the capsules were evaluated by mixing in concrete with a standard mixing process in a regular drum concrete mixer. Twenty capsules from each of the 12 manufactured gravel-level groups equivalent to a volume fraction of 1.8% were added and mixed for 5 min to ensure enough physical impact and abrasion. Immediately after the mixing process, the entire mixture was washed on a sieve with a mesh opening size of 4.76 mm to clear cement slurry and sand from the capsule shells. Then, the capsules were separated from the aggregates followed by a precise inspection of the integrity and leakage. In this study, two parameters were determined to evaluate the survivability of capsules during concrete mixing. The ratio of intact capsules to initially mixed capsules was considered the intact ratio, whereas the intact capsules without leakage were considered active capsules and were used to determine the survival ratio.

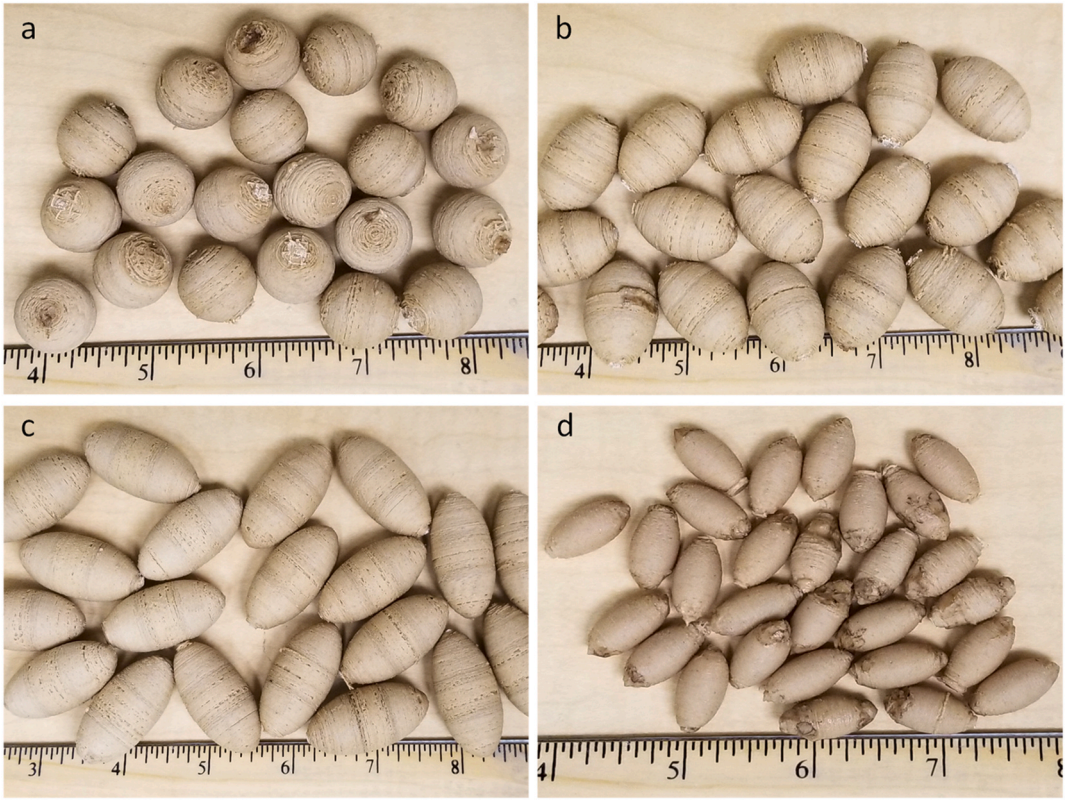

Fig. 1. Selected lignin capsules (a) G1, (b) G2, (c) G4, and (d) G6 (note: the measurements shown in the scale are in centimeters).

2.3.2. Micro-tensile test

To validate the hypothesis of switchable properties of the lignin capsules and understand the rupture behavior of the aged capsule shells in a simulated environment inside a concrete matrix, the degradation of lignin inside the simulated pore solution of concrete was assessed by performing a micro-uniaxial tensile test on the dogbone specimens using a dynamic mechanical analyzer (DMA) Q800 from TA instruments. The degradation of the dogbone specimens was achieved by soaking the gage area of the specimens with a paper towel saturated with the pore solution (see Fig. 2a and b). The soaking time of 1 h and 3 h were used to assess the degradation in strength and stiffness as compared to the untreated control specimens. As shown in Fig. 2c and d, the micro-tensile test was conducted by fixing the two ends of the dogbone specimens in the loading frame of the DMA with a controlled force loading procedure at a loading rate of 3 N/min. The test was performed at a temperature of 25 °C and a preload force of 0.01 N was applied prior to loading. Static

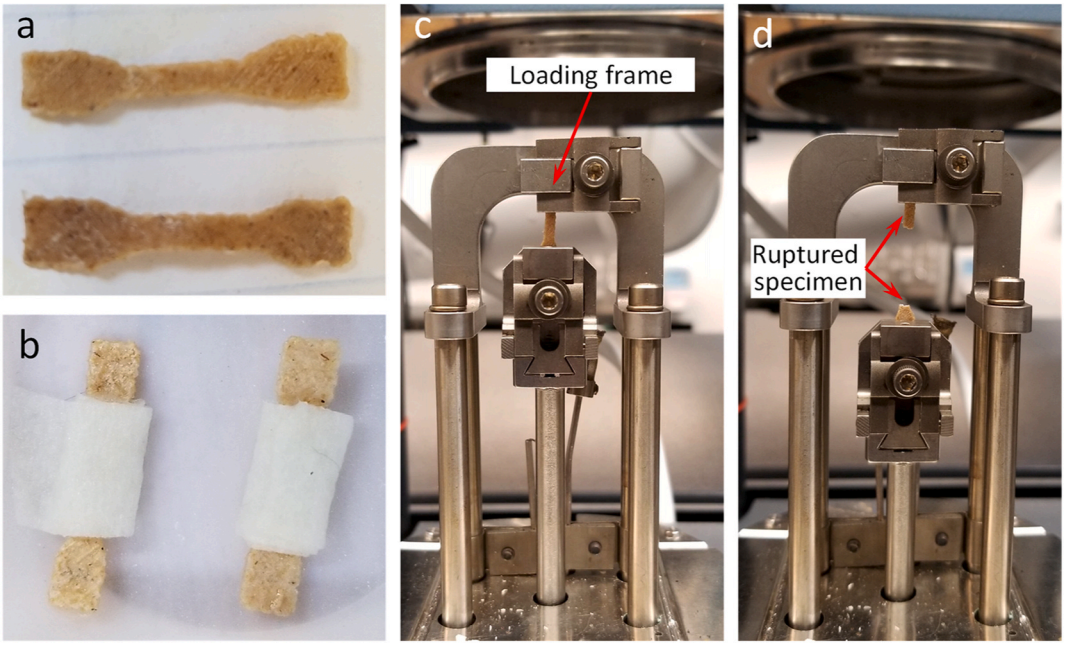

Fig. 2. (a) unaged specimens, (b) conditioning of specimens, (c) and (d) micro-tensile test setup before and after failure.

force, elongation, stress and strain were collected by the data acquisition software. The tensile strength and rupture strain were calculated as the average peak stress and the strain at rupture for each of the specimen groups. The modulus of elasticity for each specimen was calculated as the slope of the linear elastic part of each of the stress vs. strain curves.

2.3.3. Compression and split tension test

The effects of the gravel and sand level capsules on the mechanical property development of concrete and mortar were evaluated via compressive and split tensile tests after 7, 28 and 60 (90 for mortar) days. The compressive strength tests of concrete cylinders and mortar cubes were performed according to ASTM C39 [92] and ASTM C109 [93] respectively, using a PILOT compression testing machine at a constant loading rate of 126 MPa/s. The split tensile test according to ASTM C496 [94] was performed on concrete cylinders using the same machine at a loading rate of 83 MPa/s.

2.3.4. Thermogravimetric analysis

To uncover the mechanisms of the tunable properties of the lignin capsules inside the concrete, mortar, and cement paste, the degraded capsules were isolated from the specimens using a tweezer at different ages followed by a room temperature cleaning, and heating at 80 °C to remove the surface water or moisture. TGA of the collected samples was performed between 30 °C and 800 °C at a heating rate of 10 °C/min using a PerkinElmer TGA4000 under an inert nitrogen atmosphere at a flow rate of 20 mL per minute. The weight loss was recorded along with the temperature and time. The onset and burnout temperatures were determined using the modified tangent method [95] and the weight drop between a particular temperature range was ascertained to quantify the phases.

2.3.5. Self-healing efficiency

To evaluate the self-healing efficiency of the system, the mortar beams with and without lignin capsules filled with Na_2SiO_3 solution were first cracked using a 3-point flexural loading setup with a span of 203 mm (see Fig. 3). The position of the capsules inside the beam is shown in Fig. 3a. A low loading rate of 222 N/min was used, and the test was instantaneously stopped open the formation of a crack at the notch area. As shown in Fig. 3b, exudation of sodium silicate solution was observed in the crack zones indicating the effective rupture of the captures and robust healing agent release upon cracking. The crack tip passed through and reached over the capsules as shown in Fig. 3a. Due to the suction induced by the tiny crack tip, the entire crack area can be covered with exuding liquid. After creating cracks, the beams were placed under a normal room condition with a temperature of 23 ± 2 °C and relative humidity of between 30% and 35%. The evolutions of crack widths in all the beams were recorded immediately after cracking and subsequently at 1 h, 2 h, 6 h, 12 h, 24 h, 48 h, 96 h, and 120 h using a digital microscope that has a maximum magnification of 1000x and analyzed using a commercially available software ImageJ. The microscope images were converted to binary images using ImageJ and the crack area was manually segmented to analyze the change in average crack widths and crack density using a MATLAB image processing package. The images were skeletonized, and the average crack width and the total crack area were calculated using MATLAB in pixels to units of mm and mm^2, respectively. The crack density was obtained by dividing the crack area by the selected area covering the cracks. To evaluate the mechanical property recovery of the beams containing capsules, the cracked beams with and without the lignin capsule system were tested again using the same 3-point bending setup after curing for 14-days.

2.3.6. Bulk resistivity test

To evaluate the role of self-healing in the recovery of permeability, the bulk resistivity of mortar cylinders before and after cracking was measured according to ASTM C1876 [96] using RCON resistivity meter from Giatec Scientific. The cylinders were first vacuumed in a vacuum chamber with a pressure of 900–950 Pa for 3 h and then saturated in a simulated pore solution [96] under the same vacuum condition for 1 h. After the release of vacuum, the specimens were kept immersed in the pore solution for 24 h before the bulk resistivity test. The bulk resistivity of the uncracked specimens was measured by placing the cylinders between two end caps lined with conducting sponge pads and the resistance was recorded at a frequency of 1 kHz. The cylinders were then cracked by loading up to 80% of their compressive strength (as determined by the compression test) using a CONTROL compression machine in 3 cycles at a loading rate of 126 MPa/s. After each cycle, the loading was released before loading again. The development of bulk resistance of the post-cracking cylinders after 1, 3, 7 and 14 days was measured through the same vacuum saturation and resistivity test procedures as employed for the uncracked specimens.

2.3.7. Microstructure characterization

The microstructure of the 28-day aged gravel-level capsules embedded in cement paste samples was analyzed using a digital microscope and a JEOL JSM- 7401F field-emission scanning electron microscope (SEM) (JEOL USA, Peabody, MA, United States) under an accelerating voltage of 10 kV and a probe current of 9 mA, respectively. The specimens were cut from the cubic sample along the minor diameter of the capsules using a slow-speed precision saw. For the SEM test, the samples were first conditioned in a desiccator with saturated sodium hydroxide solution to remove the surface moisture and the surfaces were made conductive by sputtering deposition of a thin layer of gold using a Denton vacuum sputter coater. Energy-dispersive X-ray analysis (EDX)

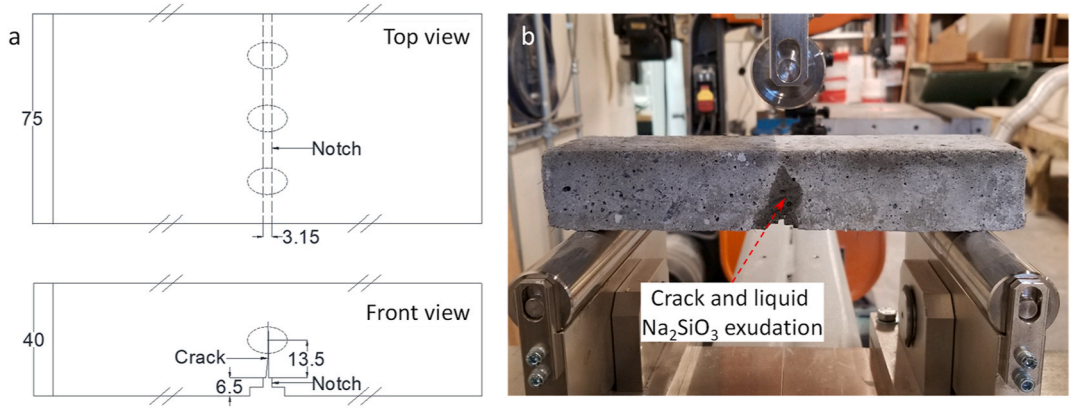

Fig. 3. (a) schematic diagrams of the beam with top view and front view, and (b) a specimen after cracking with exudation of the liquid self-healing agent (sodium silicate solution), (note: the dimensions in the schematic diagram are in mm).

under an accelerating voltage of 10 kV and a probe current of 11 mA was carried out to determine the elemental composition around the capsule-cement interface using an EDX Genesis XM2 imaging system with a 10 mm^2 Si (Li) detector and a SUTW window equipped in the SEM.

3. Results and discussion

3.1. Survivability of capsules during concrete mixing

The survivability of capsules is the first paramount important pre-requisite to achieving robust self-healing capacity in concrete. Different from other composite materials, concrete is typically manufactured by blending the raw materials via a harsh mixing process, where impact, abrasion and tear from the heavy granular gravels and sands pose a threat to the integrity and functionality of the hollow capsules with thin shells. The capsules must have enough robustness to avoid shell rupture and be capable of holding the self-healing agent. In this study, two quantities, namely intact ratio and survival ratio, have been used to assess the survivability of the synthesized lignin-based capsules during concrete mixing. One of the authors' previous studies on polylactic acid capsules has shown that geometry, aspect ratio, and shell thickness determine the survivability of the capsules. Here, all these factors were investigated for the new lignin capsules.

3.1.1. Influence of capsule size

Fig. 4 shows the intact ratio and survival ratio of the lignin capsules with a shell thickness of 0.8 mm and two aspect ratios of 1.5 and 2 and varying minor diameters from 9.5 mm to 19.05 mm. As shown in Fig. 4a, at a lower aspect ratio of 1.5, the capsules yielded a promising intact ratio between 95% and 100% for all three minor diameters (9.5 mm, 12.7 mm and 19.05). The survival ratio, however, decreased with capsule size. The small capsules in 9.5 mm and 12.7 mm exhibited survival ratios of 95% and 90%, respectively, while only 30% of the largest capsules can survive. Fig. 4b shows that for capsules with an aspect ratio of 2, an increase in minor diameter from 9.5 mm to 19.05 mm does not significantly impact the intact ratio of the lignin capsules for both capsules with 0.4 mm and 0.8 mm shell thickness. However, a 65% decrease in the survival ratio was obtained when the capsule size increased to 19.5 mm. For the two aspect ratios, the highest intact ratio of 100% and survival ratio of 95% were both yielded by the small capsules i.e., G6 and G7, which may be due to the increased surface of the larger capsules exposed to increased contact and abrasion during concrete mixing. The increased capsule size with a longer printing pathway might have also led to increased printing defects. Therefore, although a large size can deliver more healing agents, given the high intact and survival ratios, a lignin capsule with a small minor diameter is preferred.

3.1.2. Influence of aspect ratio

The aspect ratio was also found to influence the intact and survival ratios of the capsules. As is shown in Fig. 5, all the investigated capsules with minor diameters of 9.5 mm and 19.5 mm and shell thicknesses of 0.4 and 0.8 mm with varying aspect ratios from 1 to 2 can remain intact after concrete mixing. Fig. 5a shows that, for the large capsules with a minor diameter of 19.05 mm, the survival ratio drops from 60% to 30% when the aspect ratio changes from 1 to 1.5. This low survival ratio does not change with a further increase in aspect ratio. A survival ratio of 95% was yielded by the smaller capsules with a minor diameter of 9.5 mm and shell thickness of 0.8 mm, and no influence of aspect ratio was observed (see Fig. 5b). It is interesting to observe that, when the shell thickness was decreased to 0.4 mm, the small capsules exhibited the same survival ratio of 95% for the aspect ratios of 1 and 1.5, which dropped by 5% when the aspect ratio increased to 2. The comparisons indicate that the small capsules with a shell thickness of 0.4 mm are superior to large capsules with even a shell thickness of 0.8 mm. Again, this might be due to the greater surface area of the larger capsules providing more contact and abrasion from the gravel in concrete mixing. With the same minor diameter, capsules with a higher aspect ratio are preferred to carry a greater quantity of self-healing agent and capture cracks more efficiently. However, the negative impact of an extremely high elongation (i.e., an aspect ratio of 2) on capsule survivability must be taken into account.

3.1.3. Influence of shell thickness

Fig. 6 shows the effect of shell thickness on the intact and survival ratios of the lignin capsules. Based on the results above, the preferred small capsules with a 9.5 mm minor diameter and aspect ratio of 1.5 and 2 were focused on in this section. It was observed that an increase in shell thickness does not result in improved survivability. As shown in Fig. 6a, at an aspect ratio of 1.5, the capsules with shell thickness of 0.4 and 0.8 showed the same intact and survival ratios of 100% and 95%, respectively. However, the intact ratio was found to decrease by 5% and 10%, respectively, as the shell thickness increased to 1.2 mm and 2.0 mm, except for 1.6 mm shell thickness (G11). A more significant decrease in survival ratio by 15% was observed as the shell thickness increased to 1.2 mm. Although an increased survival ratio was yielded by further increased shell thickness to 1.6 mm and 2.0 mm, their survivability is still lower than that of the capsules with thinner shells (0.4 mm and 0.8 mm). This may have occurred from the weak spots in the shell created due to irregularities in between the multiple layers.

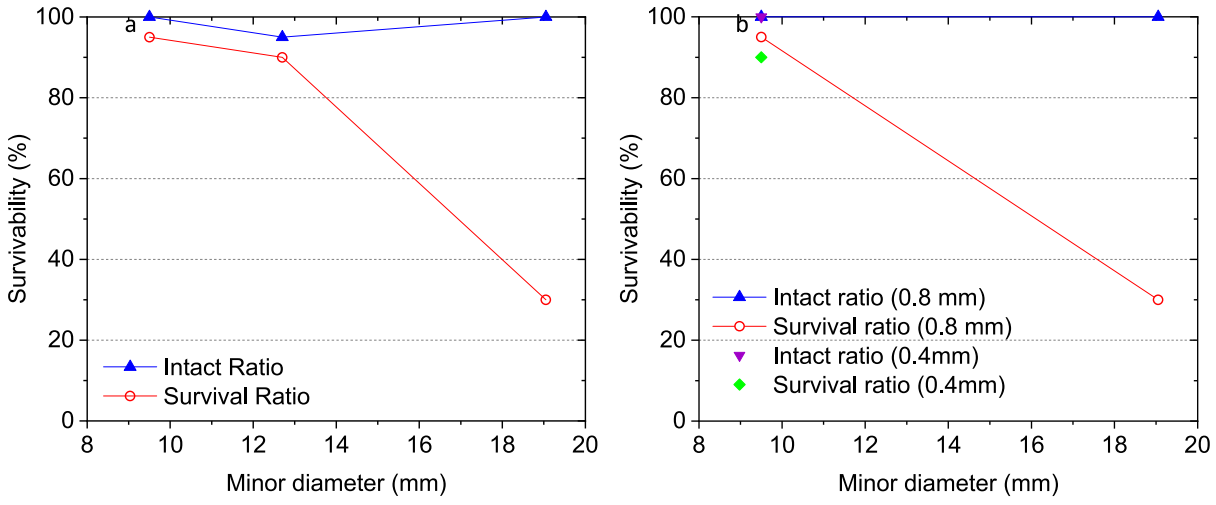

Fig. 4. Intact ratio and survivability ratio of capsules having: (a) aspect ratio of 1.5; and (b) aspect ratio of 2.

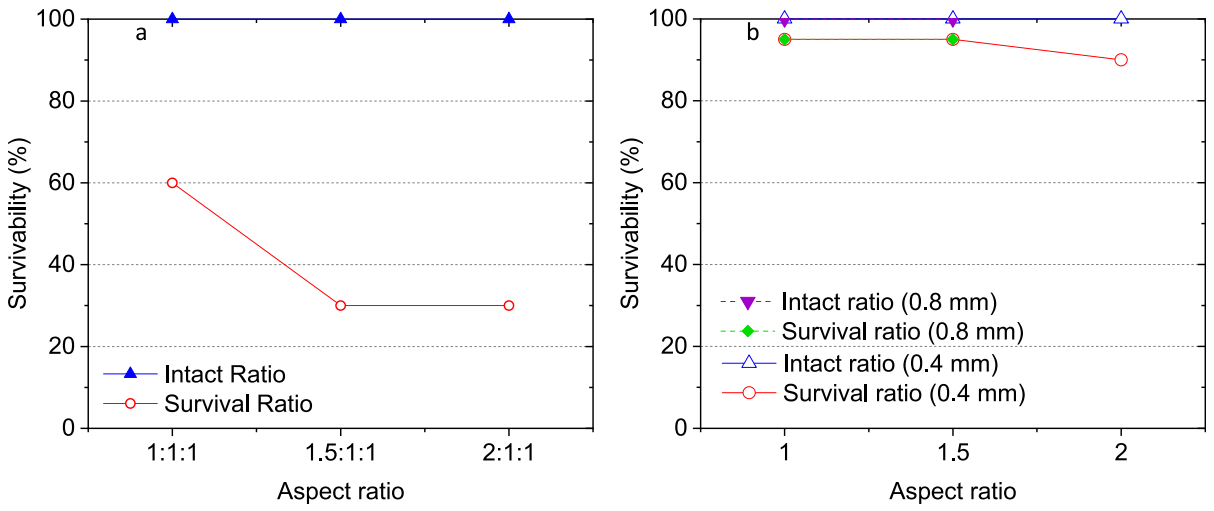

Fig. 5. The influence of aspect ratio on the intact and survival ratios of lignin capsules with: (a) minor diameter of 19.05 mm and thickness of 0.8 mm, (b) minor diameter of 9.5 mm and thicknesses of 0.8 mm and 0.4 mm.

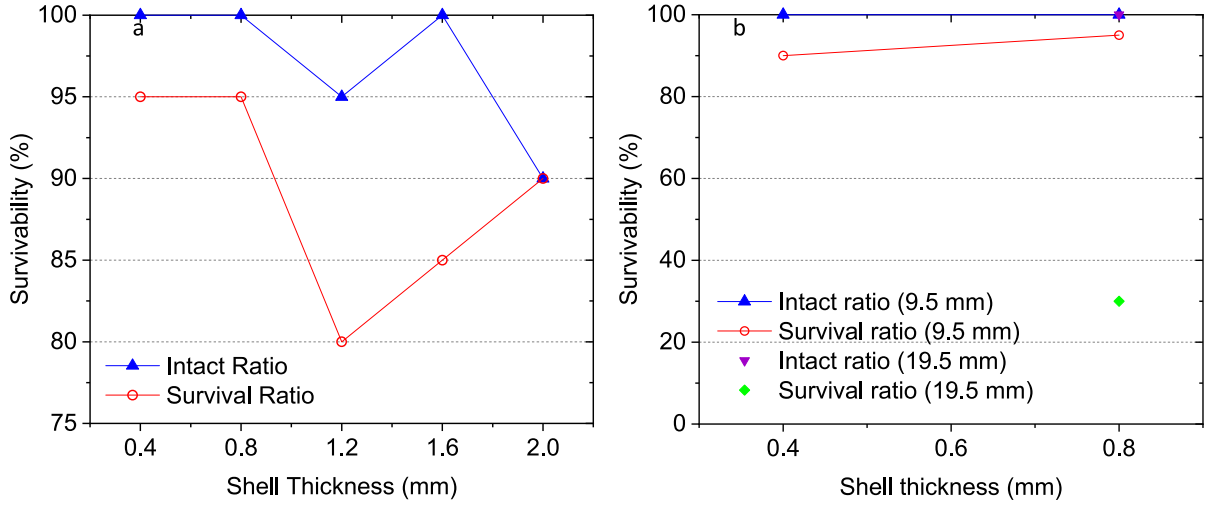

Fig. 6. Influence of shell thickness on the survivability of lignin capsules with aspect ratios of (a) 1.5 and (b) 2.

Furthermore, with the same dimension, the inner space of the hollow capsules decreases with shell thickness and hence less healing agents can be delivered. The results in Fig. 6b indicate that, at a higher aspect ratio of 2, the same intact ratio (100%) and a lower survival ratio (90%) were yielded by the capsules with a shell thickness of 0.4 mm, while the survival ratio decreased to 30% when the minor diameter was increased to 19.5 mm at a shell thickness of 0.8 mm. Based on these observations, it can be concluded that the small capsules having a minor diameter of 9.5 mm, an aspect ratio of 1.5, and a shell thickness of 0.4 mm (G8) have the maximum intact (100%) and survivability ratio (95%). Although a similar performance was obtained from G7 and G9, a higher shell thickness decreases the efficiency of capsules in reserving and delivering self-healing agents and consumes more materials in capsule synthesis. Furthermore, with the same survivability, a thinner shell will trigger a more robust rapture efficiency of the capsule upon concrete cracking to release the healing agent. Therefore, G8 and the sand-level capsules (S1) were focused on for further investigations into compatibility and self-healing capability.

3.2. Degradation behavior of lignin capsules

3.2.1. Degradation in simulated pore solution

As a key innovation of the lignin-based capsules of this study, the degradation of lignin in the cementitious environment is leveraged to achieve tunable properties, i.e., high survivability during concrete mixing and high rupture efficiency upon concrete cracking. To verify this assumption, the degradation in tensile strength of the lignin shell exposed to a simulated concrete pore solution at room temperature was evaluated by carrying out a micro-tensile test on dogbone specimens. Fig. 7a shows the stress vs. strain behavior of the lignin dogbone specimens at both unaged state and after being treated in the simulated pore solution for 1 and 3 h. The stress-strain curves of the unaged specimens show a linear variation of stress and strain indicating an elastic response up to a stress of 6 MPa, beyond which the specimens showed inelastic behavior up to failure. The differences in the stress-strain behavior of the unaged specimens may have been due to small imperfections in the gage region of the specimens resulting from 3D printing. In the presence of the alkaline solution, the influence of the small imperfections was reduced and the aged capsule shells with decreased strength and deformation capacity showed lower variation in the stress and strain curves. The specimens treated in simulated pore solution for 1 and 3 h

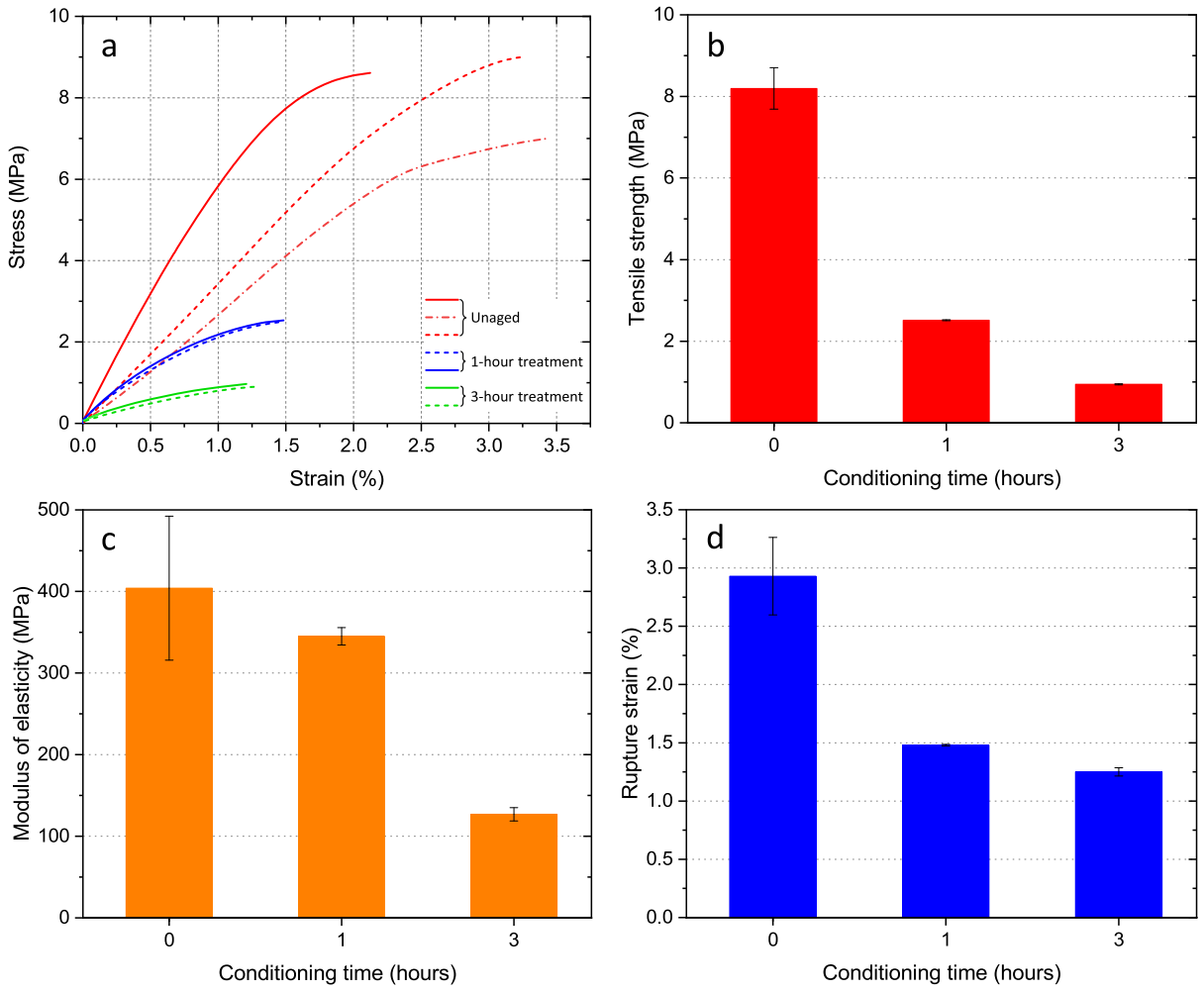

Fig. 7. Degradation of lignin in pore solution with time: (a) stress-strain curves from the micro-tensile tests and evolutions of (b) tensile strength, (c) Modulus of elasticity and (d) rupture strain.

showed elastic response for up to 0.45 MPa and 0.23 MPa, respectively, with lower slopes indicating the degradations in tensile resistance and stiffness. Among the three groups, the unaged samples exhibited the highest peak load, which decreased dramatically with the time of pore solution treatment. As shown in Fig. 7b, the control group without treatment showed the maximum tensile strength of 8.2 MPa. After 1 h and 3 h of soaking in the concrete pore solution, the strength decreased by 69.3% and 88.5%, respectively. Although this treatment is more aggressive than the real condition, the results provide an indication of the efficient degradation of the lignin-based capsule shell in concrete. After 1 and 3 h of conditioning, the aged specimens exhibited 14.6% and 68.6% lower modulus of elasticity, respectively (see Fig. 7c). Compared with the unaged controlled group, the ultimate strain at rupture was found to decrease by 49.5% and 57.3% after being conditioned for 1 and 3 h, respectively (see Fig. 7d). The decreases in tensile strength and rupture strain were more profound during the first hour of exposure to pore solution than the changes in the subsequent 2 h. This reveals the highly efficient property tunability of the lignin capsules, which is desirable for healing early-age concrete cracks. The degradation behavior of the lignin capsules in actual concrete and mortar environment was investigated (see the sections below) to further test this hypothesis.

3.2.2. *Degradation of gravel-sized capsules in concrete*

In addition to the high survivability, efficient rupture of the capsules, i.e., a tunable property, is the second prerequisite to trigger robust self-healing action in concrete. This property switchability of the lignin capsules was evaluated by the phase evolution of the capsules extracted from the concrete matrix at 7, 28, and 60 days via TGA. Fig. 8a and b shows the weight loss thermogravimetry and the derivative thermogravimetry (DTG) curves of the lignin capsules as functions of temperature, respectively. The unaged capsules showed a two-step degradation: the first weight loss from 308 °C to 362 °C, which is the degradation temperature range of lignin, shows a weight drop of 58.6%, while the second weight drop of 18.6% between 392.2 °C and 422.5 °C is attributed to the biopolymers (polylactic acid) mixed in the filament for printability improvement. It is worth noting that both the lignin matrix and the polylactic acid additive are alkaline degradable. After a 7-day immersion in concrete, the lignin capsules showed a weight loss in 3 stages: the first two weight losses for temperature ranges of 230–276.4 °C and 300–330.1 °C are attributed to the decomposition of lignin, and the second weight drop from 379 to 421.9 °C is due to polylactic acid. The reduction in the onset temperature of lignin from 308 °C to 230 °C indicates a decrease in thermal stability induced by the formation of soluble lignin and depolymerization in the presence of alkalis, which can decrease the content of C–C linkages [97]. The 2-stage degradation of lignin after 7 days indicates partial depolymerization, which was completed after 28-days as seen from a single broad weight loss with a similar onset temperature. The contents of lignin and polylactic acid were decreased by 49.4% and 14.5%, respectively. At later ages, the onset temperature of lignin remained similar to that observed from the 7-day sample. After 28 and 60 days, lignin degradations were

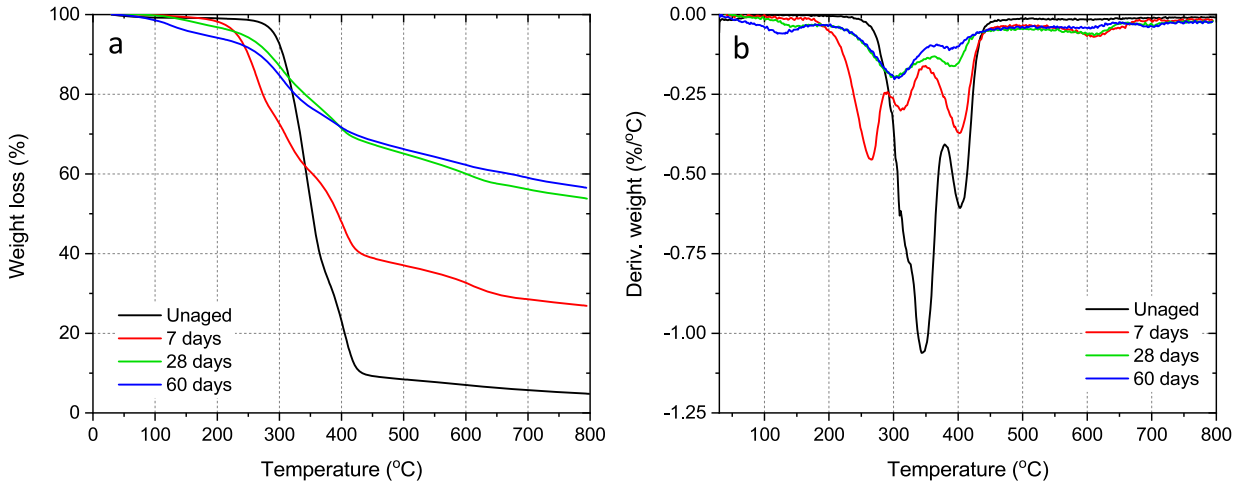

Fig. 8. (a) TGA and (b) DTG of unaged capsules and aged capsules extracted from concrete after 7, 28, and 60 days.

increased to 57.6% and 58.3%, respectively. A small amount of hydrated cement paste adhered to the surface or migrated into the shells (even after cleaning) was also observed from the extracted capsules indicated by the slight weight drops in the characteristic temperature ranges of calcium silicate hydrate (C–S–H), portlandite, and calcite. Compared with the authors' previous study [42], the main difference between the lignin capsules and that synthesized from pure PLA lies in the rate of degradation: the lignin exhibits a higher early-age degradation rate, which is almost 4 times that of the PLA at 28 days.

3.2.3. Degradation of sand-sized capsules in a mortar matrix

To understand the property tunability of the sand-level capsules in the matrix of mortar, TGA was conducted on the extracted capsule shells after an immersion of 7, 28, 90 and 120 days. Fig. 9a and Fig. 9b show the TGA and DTG curves of the unaged and aged lignin capsules inside mortar cubes cured in saturated lime solution at 23 °C. It can be seen that, after 7 days, the onset and burnout temperature of the lignin decreased to 268 °C and 318.4 °C, respectively, due to depolymerization in the alkaline mortar matrix, which is consistent with the observation for the gravel-level capsules in concrete. However, a lower degradation rate was observed from the sand-level capsules. After 7 and 28 days, the degrees of degradation of the sand-level capsules in mortar are 16.8% and 14.3% lower than that of the gravel-sized capsule. This might be due to two reasons: (i) the difference in the alkalinity between concrete and mortar, and (ii) the smaller surface area of the sand-level capsules leading to less effective contact area and a lower possibility of encountering pore solutions. Compared with the previously studied polylactic acid-based capsules, the lignin capsules exhibited 14.8% and 39.9% higher degradation rates after 7 and 28 days, respectively. Beyond 28 days, the lignin capsules did not show a significant increase in degradation, and the onset and burnout temperature decreased to 240.9 °C and 328.1 °C, respectively, after 120 days. The disappearance of the weight drop of additive indicates the full degradation of this phase at 90 days.

3.2.4. Degradation of capsules under an elevated temperature

To understand the degradation rate of the lignin capsules under a thermal condition, such as the core part of a massive concrete structure, TGA was performed on the capsule shells extracted from a cement paste in a saturated lime solution at an elevated temperature of 50 °C. The TGA and DTG curves of the capsules are shown in Fig. 10a and b, respectively. After 7 days, the onset temperature of the lignin degradation was reduced to 244.8 °C, while the burnout temperature decreased to 307.14 °C, which is lower than that observed from the embedded capsules at room temperature. This might be due to the accelerated depolymerization of lignin under the elevated curing temperature. It is interesting to note that the degradation rate was not increased appreciably under higher temperatures and a single broad weight loss between 290.9 °C and 374.7 °C was observed after 28 days. After being conditioned for 90 days, 48.6% capsule was degraded, which is 9.7%

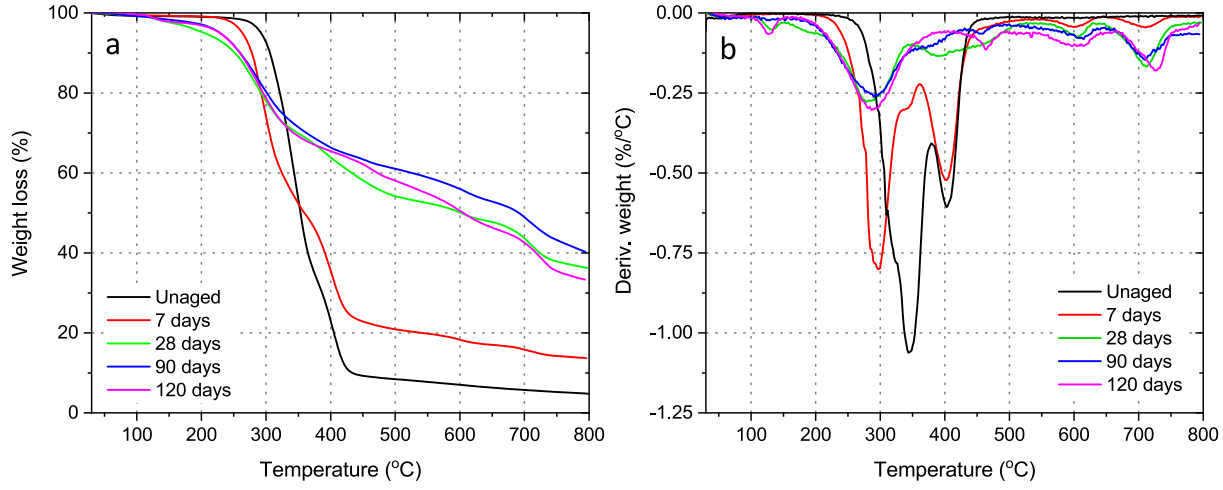

Fig. 9. (a) TGA and (b) DTG of unaged capsules and aged capsules extracted from mortar after 7, 28, 90, and 120 days.

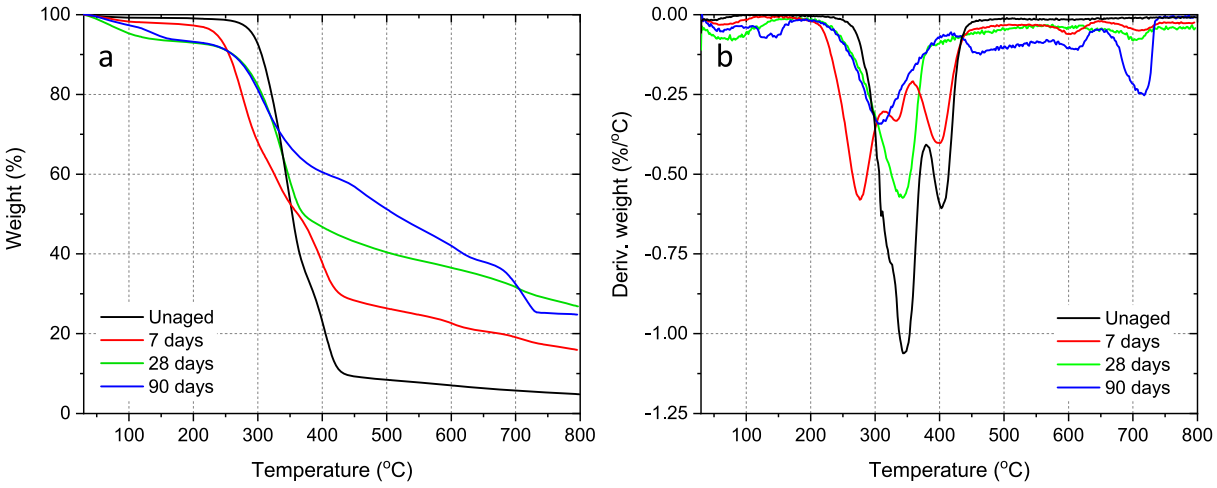

Fig. 10. (a) TGA and (b) DTG of unaged capsules and aged capsules extracted from cement paste cured at 50 °C after 7, 28, and 90 days.

lower than the 60-day capsule degradation in concrete conditioned under room temperature but 16% higher than the degradation degree of polylactic acid capsules in the same condition. The onset and burnout temperatures of the lignin capsule shell were further decreased to 268.6 °C and 352.2 °C, respectively, after 90 days of conditioning. The onset and burnout temperatures as well as the degradation degrees of the capsules under different curing conditions are summarized in Table 5.

3.3. Mechanical compatibility of the lignin capsules

The compatibility of the gravel-level and sand-level lignin capsules in concrete and mortar was evaluated by carrying out compressive and tensile strength tests on concrete cylinders and mortar cubes, respectively. The concrete contains 5 vol% G8 capsules, while the mortar is incorporated with 2 vol% S1 capsules.

3.3.1. Influence of gravel-sized capsules on concrete strength

Fig. 11a and b shows the influence of the gravel-level lignin capsules on the developments of concrete compressive strength and splitting tensile strength, respectively. As shown in Fig. 11a, by incorporating 5 vol% capsules, the 7-day, 28-day and 60-day compressive strength of concrete were reduced by 36.3%, 47.7% and 36.4%, respectively. This might be induced by multiple reasons: (i) the high capsule volume fraction employed in this study, (ii) the degradation of the lignin capsule creates weak zones inside the concrete matrix, and (iii) the capsules are lighter than the regular gravels and tended to move up during casting resulting in less homogeneous distribution. Nevertheless, increasing compressive strength of the concrete containing the lignin capsules with time was observed and the 60-day strength was increased to 34 MPa. Besides the continuous cement hydration, the decreased strength loss with the control group (plain concrete) might be partially due to the formation of solid products (C–S–H and calcite) from the reaction between sodium silicate (healing agent) with portlandite and CO_2. In addition to the strength evolution, as Fig. 12a and b, an effective exudation of the liquid sodium silicate was observed during cracking under compressive loading, which indicates the highly robust rupture and healing agent release efficiency of the aged lignin capsules upon concrete cracking.

The development of splitting tensile strength of concrete with and without capsules after 28 and 60 days is shown in Fig. 11b. The 28-day tensile strength of the concrete cylinder is 20.2% lower than the control group. After 60 days, the tensile strength was found to increase significantly making the tensile strength lower by only 17.6% when compared to the plain concrete. Since concrete is prone to cracking in flexure, the improvement of the tensile strength is promising. It is worth noting that the main reason for the decreased compressive and splitting tensile strength of concrete is the high-volume fraction of capsules employed in this study. The high number of capsules might decrease the homogeneity of the concrete mixture and induce stress concentrations resulting in local spalling or end rolling in the concrete cylinders under mechanical loadings as shown in Fig. 12a to c. Previous studies have also shown that an adverse effect on concrete strength and Young's modulus can be generated when the capsule volume fraction reaches 5%. The detrimental effect can be suppressed by decreasing the capsule volume fraction to 2%, while the self-healing capacity can also be concomitantly

Table 5
Summary of thermogravimetric analysis results.

Sample	Matrix (temperature)	Age (days)	Onset Temperature, T_d (°C)	Maximum Degradation Temperature (°C)	Weight Loss (%)	Degradation (%)
Unaged	–	0	308.0	422.5	77.2	–
Aged capsules	Concrete (23 °C)	7	230.7	421.9	45.5	31.7
		28	259.1	412.8	19.7	57.6
		60	263.9	424.5	18.9	58.3
	Mortar (23 °C)	7	268.2	426.0	62.4	14.9
		28	241.1	464.1	33.9	43.3
		90	237.5	348.0	27.9	49.3
		120	240.9	328.1	26.8	50.4
	Cement paste (50 °C)	7	244.8	422.3	54.1	23.1
		28	290.9	374.7	47.8	29.4
		90	268.6	352.2	28.6	48.6

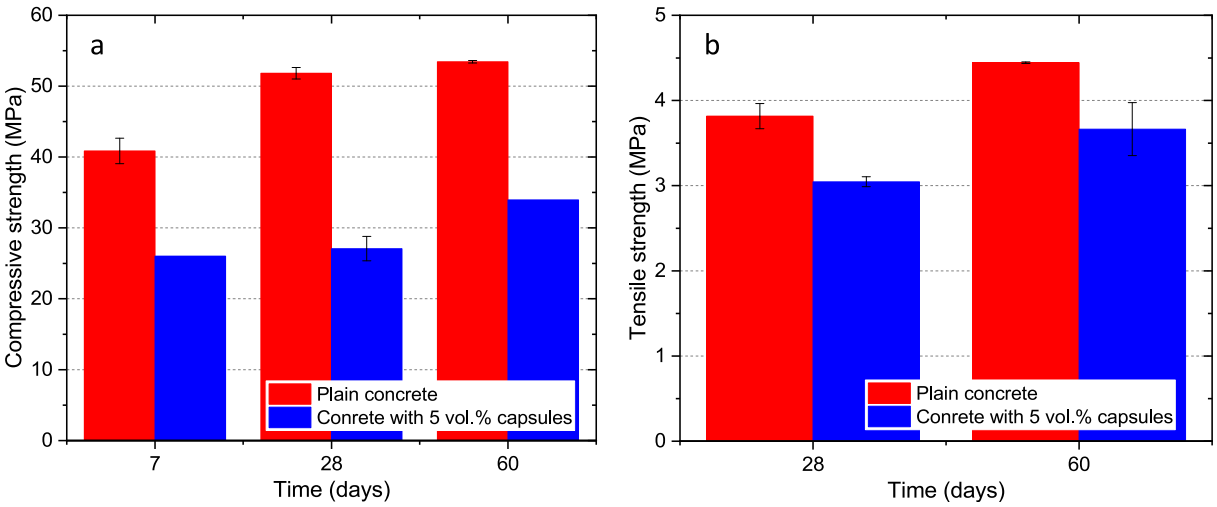

Fig. 11. Development of (a) compressive and (b) splitting tensile strength of concrete.

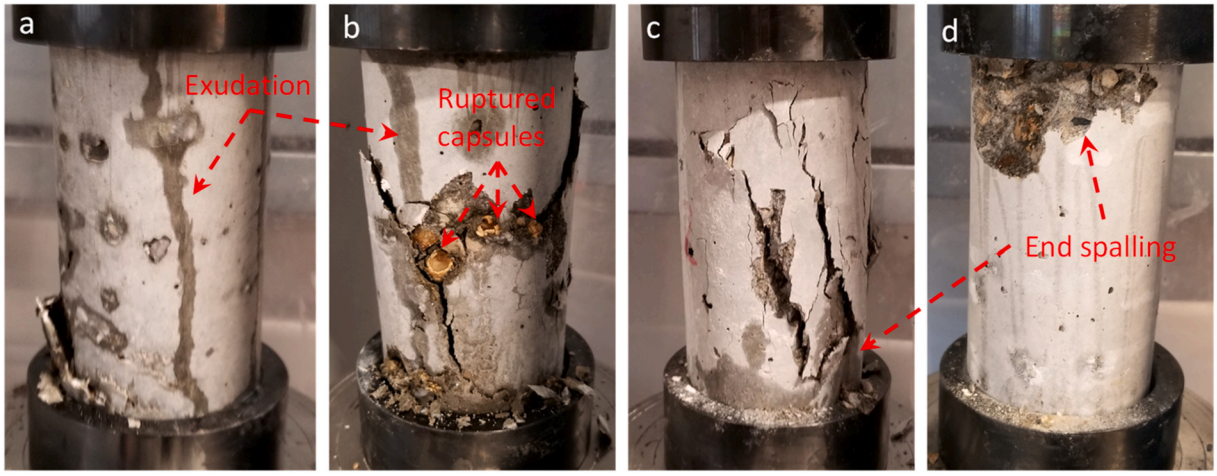

Fig. 12. Concrete cylinders under compression: (a, b) cracking and exudation of healing agent from ruptured capsules, and (c, d) end spalling.

reduced [98]. As shown in Fig. 16, the fiber-reinforced mortar beams with three embedded G8 capsules over the notch yielded comparable first cracking strength when compared with the plain concrete beams, which is promising since concrete is susceptible to flexural cracking. Further studies are necessary to determine the optimum dosage of capsules to achieve efficient self-healing without compromising the mechanical properties of concrete.

3.3.2. *Influence of sand-sized capsules on mortar strength*

The impact of the sand level capsules at a lower volume fraction of 2% on the compressive strength of mortar cured in saturated lime solution at room temperature is shown in Fig. 13. It was found that the incorporation of the lignin capsules lowers the 7-day mortar strength by 14.4%. A similar phenomenon was also observed from polylactic acid capsule in the author's previous study [42]. It is interesting to see that the overall strength development of the mortar is significantly improved compared with the case of concrete containing gravel-level capsules. At 28-days, the strength of mortar containing S1 capsules is comparable with the control group (plain mortar). A slower strength gain was yielded from 28 days to 90 days. As a result, the 90-day strength of the mortar with capsule is 12.7% lower than the plain mortar, which might be due to the degradation of the lignin capsules and the fact that the sand level capsules are still larger than most of the sand particles used in the mortar. The improvement in strength gain of the mortar outperforming

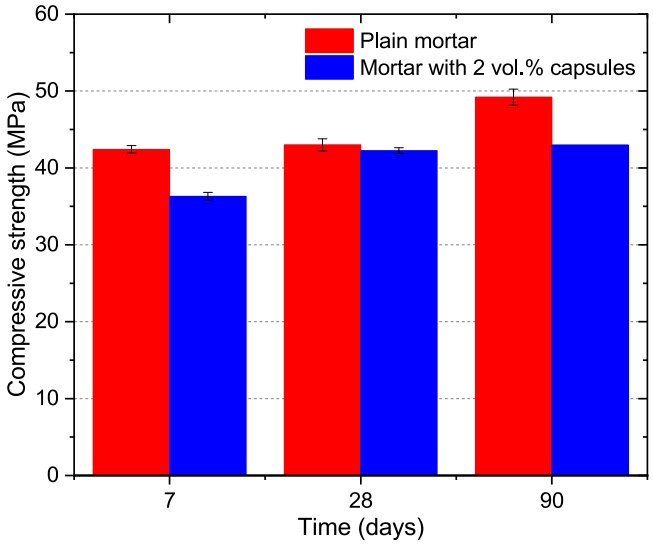

Fig. 13. Development of compressive strength of mortar containing sand-level capsules.

concrete specimens might be due to the lower volume fraction of the sand-level capsules of 2%, which is much lower than that of the gravel-level capsules in concrete (5%). Furthermore, the smaller size of the sand-level capsules can create fewer voids with a less detrimental effect on the matrix strength. These observations indicate acceptable compatibility of the sand-level lignin capsules in the mortar mix, which is in accordance with previous investigations [42,98,99].

3.4. Self-healing and property recovery efficiency

3.4.1. Crack self-healing capacity

The crack healing capability of the lignin capsule-based self-healing system was evaluated by monitoring the crack closure behavior of post-cracking fiber-reinforced mortar beams. After creating a microcrack in each bottom notch area manifested by a sharp drop in load and the exudation of the self-healing fluid, the cracks were immediately measured under a digital microscope followed by periodic

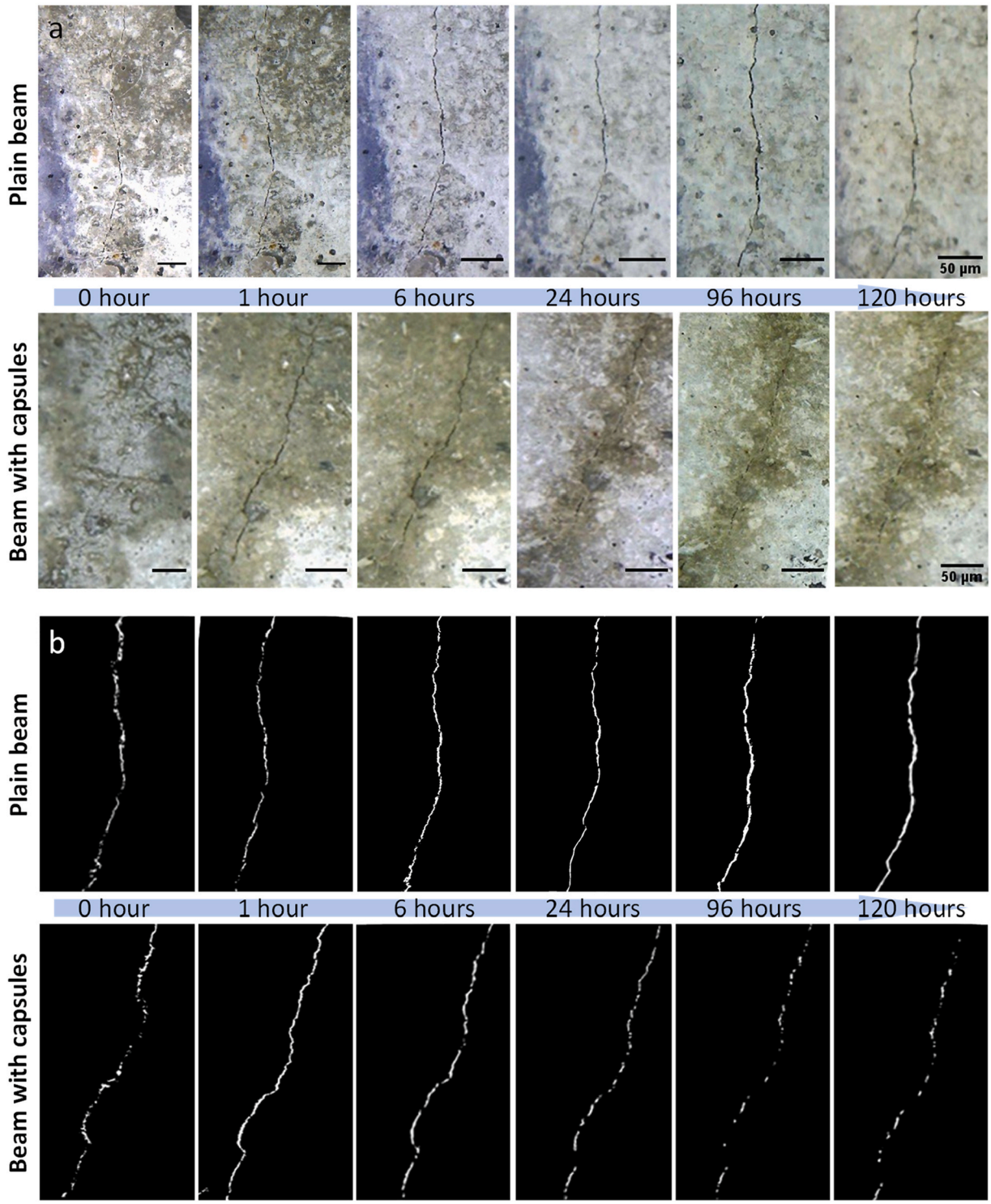

Fig. 14. Evolution of the crack width in mortar beams with and without lignin capsules: (a) original images, and (b) binary images after processing (the scale bar is 50 μm).

measurements in the next 120 h. Fig. 14a shows a comparison of the crack width at selected periods of the specimens with and without lignin capsules. The beam containing lignin capsules filled with sodium silicate solution showed exudence of the liquid from the crack immediately after the crack initiation. The crack was progressively closed due to the precipitation of C–S–H derived from the reaction between sodium silicate and portlandite, as well as the hardening of sodium silicate itself, whereas the control beam did not show crack closure even the continuous hydration of cement likely exists in this young mortar matrix. To obtain an accurate determination of the cracks and progressive crack-healing efficiency, the digital images were further quantified by an imaging processing toolbox in MATLAB after preliminary processing via ImageJ software. Fig. 14b shows the filtered binary images corresponding to the images in Fig. 14a with progressive changes in crack width and area, which were further analyzed using MATLAB to obtain average crack width and cracking density. A clear decrease in the crack width and area in the beam containing lignin capsules was observed, which indicates the successful closure of cracks via filling with sodium silicate solution and its hardening and reaction with the hydrated cement over time, whereas the plain beam showed a slight increase in crack size.

The change in the average crack width and cracking density of the beams with and without capsules is shown in Fig. 15a and b, respectively. The control beam showed no crack closure but increases of 19.5% and 8.75% in average crack width and cracking density, respectively, after 6 h. Thereafter, the average crack width and crack density of the control beam increased steadily and resulted in a maximum increase of 51.4% and 31.1%, respectively. This might be due to the self-weight of the beam as the specimens were horizontally placed on two vertical supports at the beam ends with a span that generates a mild flexural load widening the cracks on the downward cracked surface. However, under the same condition, the self-healing capsules were able to reduce the average crack width and cracking density by up to 64.3% and 84%, respectively. During the first hour, a sharp decrease in average crack width by 43.6% was observed, which is more significant in the reduction of cracking density (by 63%). This indicates the rapid crack healing capacity of the developed self-healing system, which is due to the efficient release of the sodium silicate solution from the lignin capsules (see the wet area around the cracks in Fig. 14a), and its quick hardening and reaction with the hydration cement phases in the crack zones. The successful and rapid crack closure indicates the feasibility of using the proposed self-healing system in concrete to achieve robust self-repairing capacity.

3.4.2. Strength recovery

The efficiency of mechanical property recovery of the self-healing system was evaluated by monitoring the restored flexural strength of the post-cracking beams after 14 days. As shown in Fig. 16, no decrease but a 0.7% increase in the first cracking strength was observed from the mortar beams containing three G8 capsules, which indicates that the presence of capsules over the predicted path of the crack propagation does not negatively influence the flexural cracking behavior of concrete. This is in agreement with the simulations by Huang and Ye [98], in which a capsule volume fraction of 2% is a safe value to eliminate the compromising effect on concrete mechanical properties. Compared with the original first cracking strength, although the size of surface cracks decreased, the plain beam showed a 45% lower ultimate strength. This may be due to the quasi-brittle behavior displayed by the fiber-reinforced beams after first cracking due to the major crack simulated at the notch as well as the high span to depth ratio of the beams. In the quasi-brittle type of failure, the first cracking strength is considered the ultimate strength, since no increase in load is observed beyond the first cracking, which is unlike the strain-hardening behavior. The regain of the first cracking strength by 55% indicates that, even with limited intrinsic self-healing capacity attributed to the continuous hydration of the unhydrated cement particles inside the cracks, the

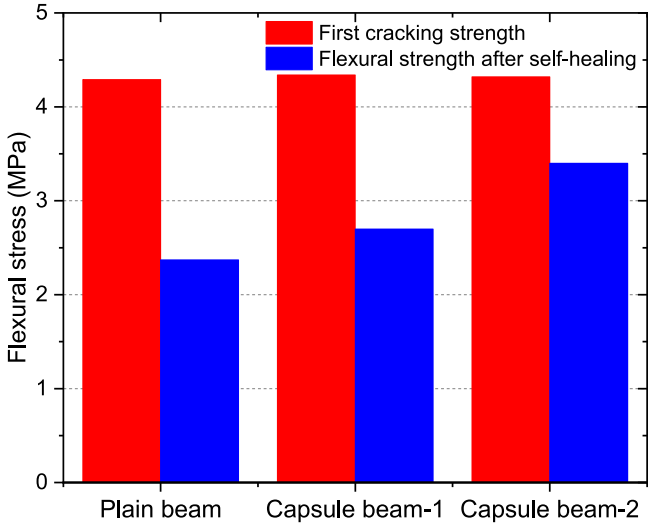

Fig. 16. First cracking strength and flexural strength of mortar beams with and without the lignin capsule system after self-healing.

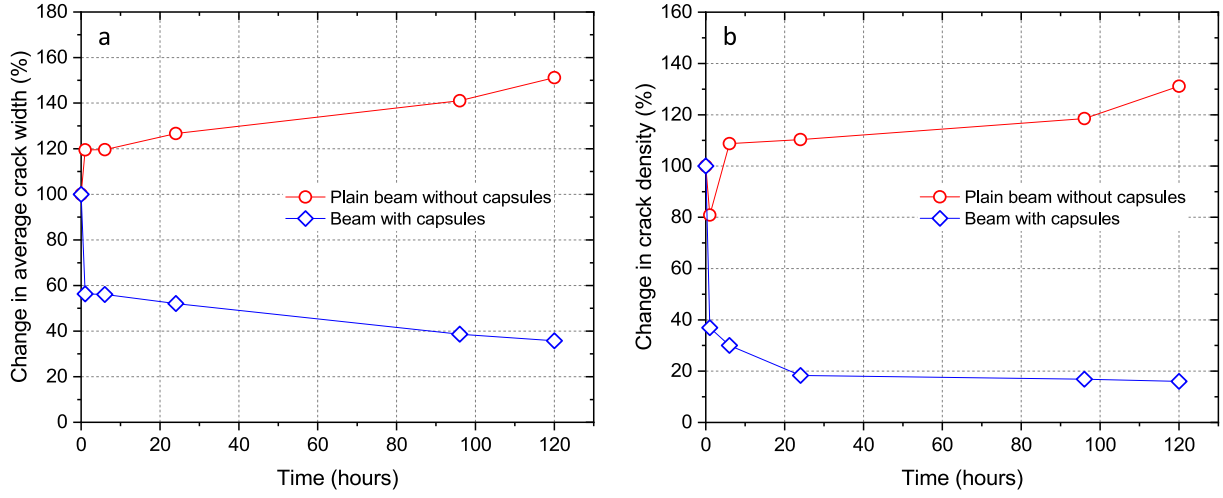

Fig. 15. Self-healing efficiency: (a) development of average crack width and (b) evolution of cracking density of mortar beams with and without lignin capsules.

fiber-reinforced mortar beams in this study exhibited quasi-brittle behavior under bending and the peak load was obtained from the first-cracking stage. It was observed that the crack created at the notch reached up to 80% of the overall depth of the beam (as shown in Fig. 3b). However, with the robustly healed cracks, the two beams with the lignin capsule system showed that the ultimate strength after crack closure was 62.2% and 78.7% of the original first cracking stress, which are 13.9% and 43.5% greater, respectively, when compared to the plain beam. This indicates that the cracks inside the damaged beams were filled with products from the reaction between sodium silicate and the cement hydrates (like portlandite) with high interfacial bonding coherence. However, a more comprehensive elucidation of the recovery of flexural, compressive and tensile strength, as well as an in-situ understanding of mechanical property evolution of the newly formed phases and the bonding strength within the crack zones under repeated cracking are desired in future works.

3.4.3. Recovery of permeability

Cracks substantially change the transport properties and increase the permeability of concrete by providing paths for external moisture and salts to migrate into concrete leading to a variety of deteriorations. Therefore, one of the most critical roles of self-healing is to suppress the crack-induced permeability increase. In this study, the efficiency of the lignin capsule-based self-healing system in recovering concrete permeability was evaluated by measuring the evolution of bulk electrical resistance. A decrease in bulk resistivity indicates the presence of a well-connected network of pores or cracks, which are filled with conducting fluid and help the flow of current. As shown in Fig. 17, before cracking, the plain cylinders showed an average bulk resistivity of 1,858.8 Ω cm. Interestingly, the incorporation of lignin-based capsules resulted in a 14.1% increase in bulk resistivity indicating a reduced permeability of the uncracked cylinders. Right after cracking, due to the formation of a network of connected paths through which current can flow, the bulk resistivity of the control and capsule-containing cylinders dropped by 4.7% and 6.3%, respectively. A continuous decrease in the bulk resistivity of the control cylinders was observed. As a result, the permeability after 72 h and 168 h is 5.3% and 7.1% higher than the original value. Agreeing well with the evolutions of crack width and strength recovery, the specimens with lignin capsules showed resistivity increases of 1.7% and 2.2% after 72 h and 168 h, respectively. This is most likely induced by the effective crack healing, which reduced the connectivity of the inner network due to the precipitations of newly formed phases. As a result, the bulk resistivity of the cylinders containing the lignin capsule-based self-healing system is 14.8% and 19.6% higher than the plain cylinder after 72 and 168 h, respectively, exceeding the original difference of the uncracked cylinders. This robust recovery of bulk resistivity further evidences the effective role of the synthesized lignin-based capsules in triggering robust crack self-healing and property recovery of concrete. It is well known that the permeability of concrete dominates its resistance against a variety of deteriorations. Therefore, it is anticipated that the developed tunable capsules can also play a positive role in improving the degradation tolerance of concrete. Further complementary investigations remain crucial in elucidating the role of this novel capsule system in optimizing the durability of cement composites, which will be the focus of an upcoming study.

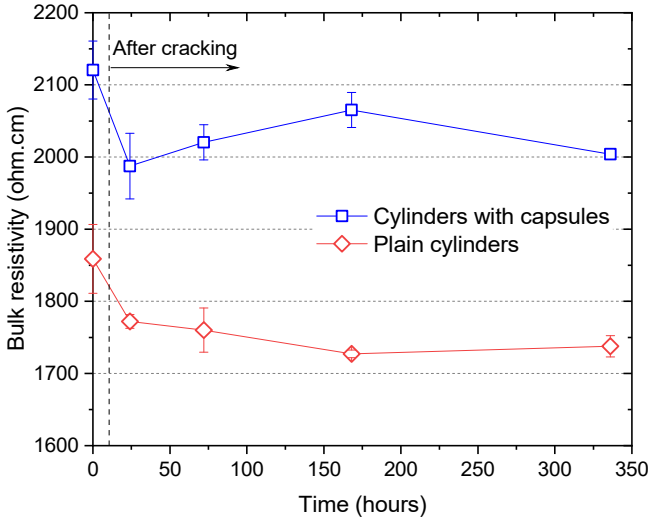

Fig. 17. Influence of lignin capsules on bulk resistivity development of mortar.

3.5. Microstructure and chemical composition analysis

The microstructure and morphology of the degraded capsules inside the cement matrix were evaluated under a digital microscope and SEM. Fig. 18a and b shows a cross-section after cutting along the minor axis of an embedded capsule under the digital microscope. From Fig. 18a, it can be seen that the capsule still maintained high integrity even with degradation. A tight interfacial bond between the capsule shell and the hydrated cement matrix is observed in Fig. 18b. The white and translucent gel-like phases inside the capsule or adhering to the inner shell wall are the sodium silicate. The SEM imaging was performed by focusing on the interfacial transition zone between the capsule and cement to elucidate the interplay between the two materials, as well as the capsule shell to understand its chemical degradation. As a local zoom of the interface in Fig. 18b and c shows an interlaced contact between the capsule shell and the surrounding hydrated cement matrix implying a strong interfacial bonding. The lignin microfibrils are partially stripped as a result of alkaline degradation (see Fig. 18d). Enlarging a portion of the interface shows the aligned micro-fibrils of the lignin capsule intercalated with cement hydration products (Fig. 18e and f). The formation of these hydrated cement phases inside the capsule shell might be a result of cement hydration products ingress into the stripped microfibrils, mineral precipitations due to the supersaturation of pore solution after infiltrating into the capsule shell wall, or the combination of these two mineralization mechanisms. The same phenomenon was observed in the author's previous study [100,101], where calcium hydroxide induced mineralization and self-mineralization due to alkaline hydrolysis of lignin in a natural fiber were identified and quantitatively characterized. The combination of these two mineralization mechanisms can substantially increase the brittleness of natural biopolymers leading to decreased tensile resistance and strain capacity. This is in line with the observations from the micro-tensile test of the lignin capsule shell (see Section 3.2.1) and explains the ease of capsule rupture in the concrete and mortar specimens under compression and tensile loads. This again evidences the great compatibility and property tunability of the synthesized lignin-based capsules in the matrix of concrete.

To further elucidate the mineralization and deposition behavior of cement hydration products in the capsule shell, EDS at the cement-capsule interface was performed to analyze elemental composition. As shown in Fig. 19a, a series of testing sites linearly distributed along a line perpendicular to the interface from the cement paste to the inner capsule was tested. The intersection between cement paste and capsule shell was defined as the origin point, from which the distances to the left cement paste and the right capsule are assigned negative and positive values, respectively. From Fig. 19b, it was found that the points in the cement paste show high atomic percentages of calcium and silica, which are the main constituents of the major hydration product C–S–H. Carbon was also detected in the cement paste region, which may be due to contaminants from specimen handling and coating. As the selected location moved away from the cement paste into the lignin capsules region, the carbon content increased steadily. This is expected since lignin is an organic biopolymer consisting of cross-linked and polymerized three monolignols (*p*-coumaryl alcohol, coniferyl alcohol and sinapyl alcohol) [102]. The amount of silicon was detected at a low level inside the

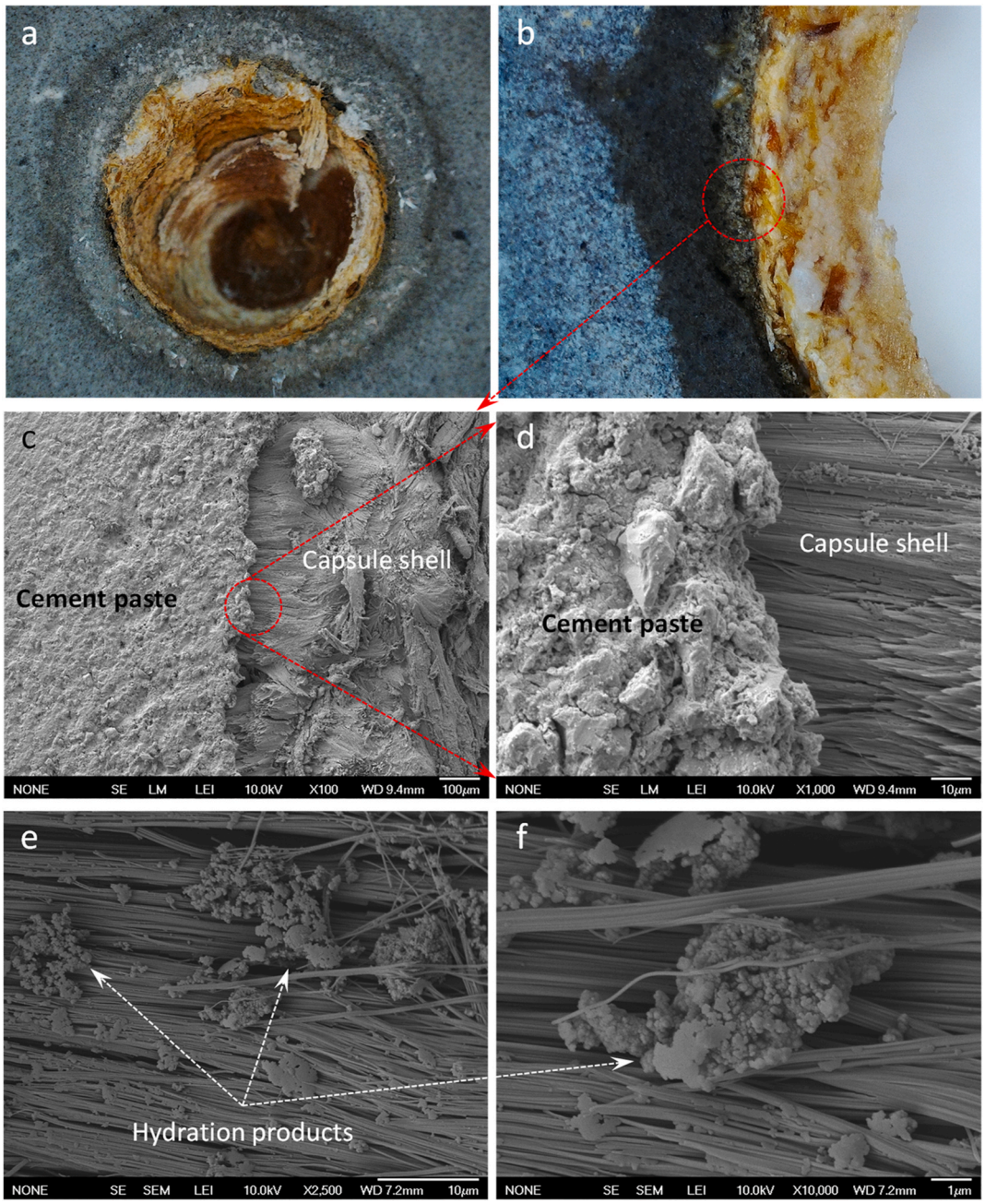

Fig. 18. Microstructure and morphology of the degraded capsules inside the cement matrix: (a) cross-section after cutting, (b) interfacial bonding between capsule wall and the cement matrix, (c, d) SEM images of the capsule-cement interface, and (e, f) aligned, stripped microfibrils of capsule shell intercalated with cement hydration products (the red circles present the spot with further enlargement, and the red arrows indicate the local zoom highlighted by the circles). (For interpretation of the references to colour in this figure legend, the reader is referred to the Web version of this article.)

capsule shell, while a high content of calcium between 16.7% and 23.3% was observed. This indicates that the capsule shell's mineralization is not induced by silicious hydrates but by calcium-rich phases like portlandite. With a further increase of distance into capsules, less calcium can be detected indicating that the mineralization is most prominent at the interface between capsule and cement, as well as inside the capsule shell. This not only reveals the reason for the tunable property of the capsule but also indicates that the healing agent can be well protected in the capsule without reaction before the self-healing action. Additional EDS acquired from the hydration products (the solid symbols in Fig. 19b) intercalated inside the capsule shell microfibrils suggested the co-existence of carbon from lignin, calcium from portlandite, and a high amount of silicon from the silicious hydrates, like C–S–H and ettringite. These observations again indicate the excellent compatibility between the lignin capsules and the surrounding cement matrix and support the future application of the lignin capsules for robust self-healing concrete.

4. Conclusions

To address the contradiction between the requirements of high survivability of capsules in the harsh concrete mixing process and the effective rupture of the capsules upon concrete cracking for effective release of healing agents into the crack zone, the present study investigated a biomass capsule system derived from lignin. Ellipsoidal capsules at both gravel and sand levels with different sizes, aspect ratios and shell wall thicknesses manufactured via 3D printing were studied. The

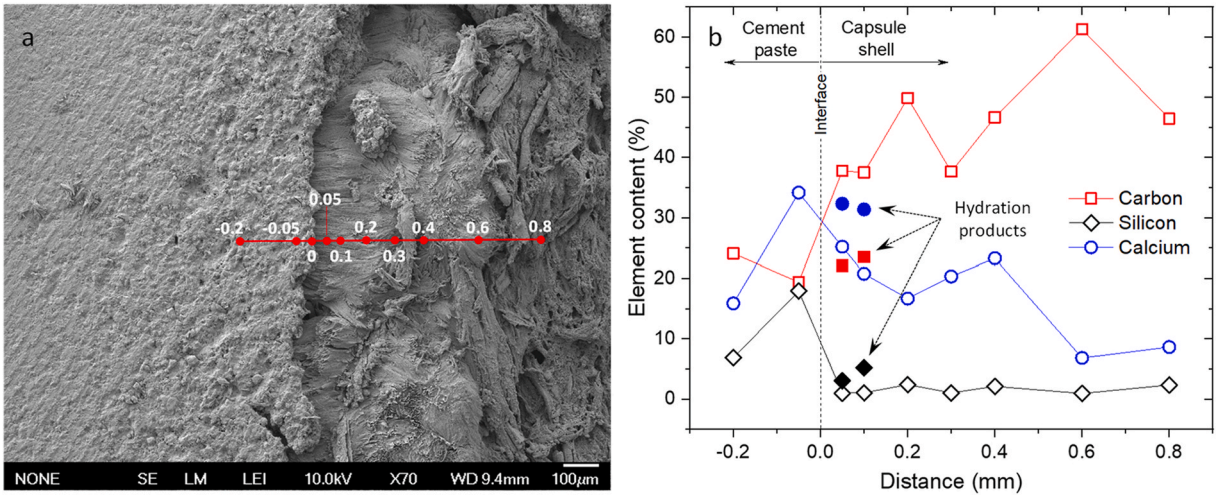

Fig. 19. Elemental analysis of the cement paste-capsule interface: (a) SEM image showing the EDX points and (b) atomic percentages of elements.

feasibility and compatibility of the lignin-based capsules with concrete were evaluated by means of survivability in concrete mixing, degradation behavior of the capsule shell material in simulated pore solution, concrete, mortar and cement paste under varying temperatures, the influence of capsules on compressive and flexural strength of concrete and mortar, self-healing efficiency of the cracks, and recovery of cracked concrete strength and permeability. The findings from this study indicate the promising potential of this biomass capsule to achieve robust self-healing capacity in concrete and pave a path for designing self-repairing concrete with various healing agents in a cost-effective and sustainable way. The following conclusions can be drawn:

1. The capsules with an aspect ratio of 1.5, a minor diameter of 9.5 mm, and shell thickness of 0.4 mm exhibited exceptional intact and survival ratios of 100% and 95%, respectively, outperforming larger capsules with thicker shells. The lower shell thickness implies less raw materials, faster manufacturing along with the capability of carrying more healing agents.
2. After being treated in concrete pore solution, the tensile strength, modulus of elasticity and rapture strain of the capsule shell material decreased by 88.5%, 57.3% and 68.6%, respectively. The capsules embedded in concrete at 23 °C exhibited a degradation degree of 57.6% after 28 days, while a lower degradation degree of 48.6% was obtained after 90 days at an elevated temperature (50 °C). This verified the tunable properties of the lignin-based capsules, in which the high initial strength ensures survivability during concrete mixing and the low strength at later ages triggers the ease of rupture upon the formation of concrete cracks.
3. The 60-day compressive and splitting tensile strength of concrete with 5 vol% gravel-level capsules was reduced by 36.4% and 17.6%, respectively. However, the 90-day strength loss of mortar containing sand-level capsules at a volume fraction of 2% was reduced to 12.7%, and a 0.7% increase in the first cracking strength was obtained from the mortar beams containing three capsules over the predicted crack propagation path, which indicates the great mechanical compatibility of the lignin capsules with concrete at an appropriate volume fraction.
4. In the presence of lignin capsules filled with a sodium silicate solution, the average crack width and cracking density were decreased by 43.6% and 63%, respectively, within 1 h of cracking. After 120 h, the healing degrees of average crack width and cracking density were further increased to 64.2% and 84% indicating the efficient crack healing performance.
5. After 14 days, the rapid and robust self-healing capacity resulted in a 78.7% first cracking strength recovery in the cracked mortar beams and a 94.5% recovery of concrete bulk resistance suggesting a significant permeability reduction.
6. The microstructural and elemental analyses show excellent interfacial bonding between the lignin capsules and the surrounding cement matrix with the migration of cement hydration products into the capsule shells, which verified the alkaline degradation and mineralization of lignin and explained the effective release of the healing agent when cracks are formed in concrete.

Declaration of competing interest

The authors declare that they have no known competing financial interests or personal relationships that could have appeared to influence the work reported in this paper.

Data availability

Data will be made available on request.

Acknowledgments

The first author (research assistant) of this study was funded by the United States National Science Foundation under award number 1935799.

References

[1] J. Cabrera, Deterioration of concrete due to reinforcement steel corrosion, Cement Concr. Compos. 18 (1) (1996) 47–59.
[2] F.U.A. Shaikh, Effect of cracking on corrosion of steel in concrete, Int. J. Concr. Struct. Mater. 12 (1) (2018) 3.
[3] S. Fan, J.M. Hanson, Effect of alkali silica reaction expansion and cracking on structural behavior of reinforced concrete beams, ACI Struct. J. 95 (1998) 498–505.
[4] E. Garcia-Diaz, J. Riche, D. Bulteel, C. Vernet, Mechanism of damage for the alkali–silica reaction, Cement Concr. Res. 36 (2) (2006) 395–400.
[5] M. Zhang, J. Chen, Y. Lv, D. Wang, J. Ye, Study on the expansion of concrete under attack of sulfate and sulfate–chloride ions, Construct. Build. Mater. 39 (2013) 26–32.
[6] A. AL-Ameeri, M. Rafiq, O. Tsioulou, Influence of Cracks on the Carbonation Resistance of Concrete Structures, Sixth International Conference on the Durability of Concrete Structures, University of Leeds, 2018, pp. 358–367.
[7] Q. Dai, K. Ng, Y. Liu, X. Yu, Investigation of internal frost damage in concrete with thermodynamic analysis, microdamage modeling, and time-domain reflectometry sensor measurements, J. Mater. Civ. Eng. 25 (9) (2013) 1248–1259.
[8] T.S.D.C. (SDC), Vision 2020 - A Vision for the Concrete Repair, Protection and Strengthening Industry, 2004.
[9] U.M. Angst, Challenges and opportunities in corrosion of steel in concrete, Mater. Struct. 51 (1) (2018) 4.
[10] H.F.W. TAYLOR, Proposed structure for calcium silicate hydrate gel, J. Am. Ceram. Soc. 69 (6) (1986) 464–467.

[11] A. Sidiq, S. Setunge, R.J. Gravina, F. Giustozzi, Self-repairing cement mortars with microcapsules: a microstructural evaluation approach, Construct. Build. Mater. 232 (2020), 117239.

[12] R.M. Andrew, Global CO2 emissions from cement production, 1928–2018, Earth Syst. Sci. Data 11 (4) (2019) 1675–1710.

[13] D. Zhu, L. Zhu, C. Philippe, D. Steven, Z. Bo, W. Yilong, C. Duo, Z. Biqing, D. Xinyu, K. Piyu, S. Taochun, G. Rui, Z. Haiwang, G. Runtao, Daily Updated Dataset of National and Global CO2 Emissions from Fossil Fuel and Cement Production, 2020.

[14] Z. Liu, P. Ciais, Z. Deng, S.J. Davis, B. Zheng, Y. Wang, D. Cui, B. Zhu, X. Dou, P. Ke, T. Sun, R. Guo, H. Zhong, O. Boucher, F.-M. Bréon, C. Lu, R. Guo, J. Xue, E. Boucher, K. Tanaka, F. Chevallier, Carbon Monitor, a near-real-time daily dataset of global CO2 emission from fossil fuel and cement production, Sci. Data 7 (1) (2020) 392.

[15] R. Guo, J. Wang, L. Bing, D. Tong, P. Ciais, S.J. Davis, R.M. Andrew, F. Xi, Z. Liu, Global CO2 uptake by cement from 1930 to 2019, Earth Syst. Sci. Data 13 (4) (2021) 1791–1805.

[16] K. Fukuyama, Y. Higashibata, Y. Miyauchi, Studies on repair and strengthening methods of damaged reinforced concrete columns, Cement Concr. Compos. 22 (1) (2000) 81–88.

[17] C.G. Karayannis, G.M. Sirkelis, Strengthening and rehabilitation of RC beam–column joints using carbon-FRP jacketing and epoxy resin injection, Earthq. Eng. Struct. Dynam. 37 (5) (2008) 769–790.

[18] T. Triantafillou, N. Plevris, Strengthening of RC beams with epoxy-bonded fibre-composite materials, Mater. Struct. 25 (4) (1992) 201–211.

[19] N. Otsuki, J.-S. Ryu, Use of electrodeposition for repair of concrete with shrinkage cracks, J. Mater. Civ. Eng. 13 (2) (2001) 136–142.

[20] J.-S. Ryu, An experimental study on the repair of concrete crack by electrochemical technique, Mater. Struct. 34 (7) (2001) 433–437.

[21] W.A. Thanoon, M. Jaafar, M.R.A. Kadir, J. Noorzaei, Repair and structural performance of initially cracked reinforced concrete slabs, Construct. Build. Mater. 19 (8) (2005) 595–603.

[22] B. Zhang, F. Gao, X. Zhang, Y. Zhou, B. Hu, H. Song, Modified cement-sodium silicate material and grouting technology for repairing underground concrete structure cracks, Arabian J. Geosci. 12 (22) (2019) 1–10.

[23] B. Dong, Y. Wang, G. Fang, N. Han, F. Xing, Y. Lu, Smart releasing behavior of a chemical self-healing microcapsule in the stimulated concrete pore solution, Cement Concr. Compos. 56 (2015) 46–50.

[24] C. Edvardsen, Water Permeability and Autogenous Healing of Cracks in Concrete, Innovation in Concrete Structures: Design and Construction, Thomas Telford Publishing, 1999, pp. 473–487.

[25] W. Ramm, M. Biscoping, Autogenous healing and reinforcement corrosion of water-penetrated separation cracks in reinforced concrete, Nucl. Eng. Des. 179 (2) (1998) 191–200.

[26] T.G. Nijland, J.A. Larbi, R.P. van Hees, B. Lubelli, M. de Rooij, Self healing phenomena in concretes and masonry mortars: a microscopic study, Proc. 1st Int. Conf. on Self Healing Materials, Springer, Dordrecht, The Netherlands, 2007, pp. 1–9.

[27] C.-M. Aldea, W.-J. Song, J.S. Popovics, S.P. Shah, Extent of healing of cracked normal strength concrete, J. Mater. Civ. Eng. 12 (1) (2000) 92–96.

[28] C. Clear, The effects of autogenous healing upon the leakage of water through cracks in concrete, 1985.

[29] S. Jacobsen, E.J. Sellevold, Self healing of high strength concrete after deterioration by freeze/thaw, Cement Concr. Res. 26 (1) (1996) 55–62.

[30] H.-W. Reinhardt, M. Jooss, Permeability and self-healing of cracked concrete as a function of temperature and crack width, Cement Concr. Res. 33 (7) (2003) 981–985.

[31] M. Şahmaran, S.B. Keskin, G. Ozerkan, I.O. Yaman, Self-healing of mechanically-loaded self consolidating concretes with high volumes of fly ash, Cement Concr. Compos. 30 (10) (2008) 872–879.

[32] T.-H. Ahn, T. Kishi, Crack self-healing behavior of cementitious composites incorporating various mineral admixtures, J. Adv. Concr. Technol. 8 (2) (2010) 171–186.

[33] M. Sahmaran, G. Yildirim, T.K. Erdem, Self-healing capability of cementitious composites incorporating different supplementary cementitious materials, Cement Concr. Compos. 35 (1) (2013) 89–101.

[34] A.E.M. Abd_Elmoaty, Self-healing of polymer modified concrete, Alex. Eng. J. 50 (2) (2011) 171–178.

[35] T. Katsuhata, Y. Ohama, K. Demura, Investigation of microcracks self-repair function of polymer-modified mortars using epoxy resins without hardeners, in: Proceedings of 10th International Congress on Polymers in Concrete, Honolulu, HI, USA, 2001, pp. 23–25.

[36] Y. Ohama, Recent progress in concrete-polymer composites, Adv. Cement Base Mater. 5 (2) (1997) 31–40.

[37] B.R. Reddy, F. Liang, R. Fitzgerald, Self-healing cements that heal without dependence on fluid contact: a laboratory study, SPE Drill. Complet. 25 (2010) 309–313, 03.

[38] X. Yuan, W. Sun, X. Zuo, H. Li, The crack self-healing properties of cement-based material with EVA heat-melt adhesive, J. Wuhan Univ. Technol.-Materials Sci. Ed. 26 (4) (2011) 774–779.

[39] M.M. Pelletier, R. Brown, A. Shukla, A. Bose, Self-healing concrete with a microencapsulated healing agent, Kingston, RI, United States, 2011 [Report].

[40] P. Giannaros, A. Kanellopoulos, A. Al-Tabbaa, Sealing of cracks in cement using microencapsulated sodium silicate, Smart Mater. Struct. 25 (8) (2016), 084005.

[41] A. Kanellopoulos, P. Giannaros, A. Al-Tabbaa, The effect of varying volume fraction of microcapsules on fresh, mechanical and self-healing properties of mortars, Construct. Build. Mater. 122 (2016) 577–593.

[42] A. Sinha, Q. Wang, J. Wei, Feasibility and compatibility of a biomass capsule system in self-healing concrete, Materials 14 (4) (2021) 958.

[43] Y.Ç. Erşan, E. Hernandez-Sanabria, N. Boon, N. De Belie, Enhanced crack closure performance of microbial mortar through nitrate reduction, Cement Concr. Compos. 70 (2016) 159–170.

[44] H.M. Jonkers, A. Thijssen, K. van Breugel, Bacteria mediated remediation of concrete structures, in: Proceedings of the Second International Symposium on Service Life Design for Infrastructures. Delft, The Netherlands, 2010, pp. 833–840.

[45] H.J. Kim, H.J. Eom, C. Park, J. Jung, B. Shin, W. Kim, N. Chung, I.-G. Choi, W. Park, Calcium carbonate precipitation by Bacillus and Sporosarcina strains isolated from concrete and analysis of the bacterial community of concrete, J. Microbiol. Biotechnol. 26 (3) (2016) 540–548.

[46] K. Van Tittelboom, N. De Belie, W. De Muynck, W. Verstraete, Use of bacteria to repair cracks in concrete, Cement Concr. Res. 40 (1) (2010) 157–166.

[47] J. Wang, K. Van Tittelboom, N. De Belie, W. Verstraete, Use of silica gel or polyurethane immobilized bacteria for self-healing concrete, Construct. Build. Mater. 26 (1) (2012) 532–540.

[48] C. Jin, R. Yu, Z. Shui, Fungi: a neglected candidate for the application of self-healing concrete, Front. Built. Environ. (2018) 62.

[49] R. Konwarh, S.B. Palanisamy, P.K. Jogi, A mini review on prospects and challenges of harnessing fungi for concrete-crack healing, Material Sci.Res. India 17 (2) (2020) 117–128.

[50] J. Luo, X. Chen, J. Crump, H. Zhou, D.G. Davies, G. Zhou, N. Zhang, C. Jin, Interactions of fungi with concrete: significant importance for bio-based self-healing concrete, Construct. Build. Mater. 164 (2018) 275–285.

[51] R.R. Menon, J. Luo, X. Chen, H. Zhou, Z. Liu, G. Zhou, N. Zhang, C. Jin, Screening of fungi for potential application of self-healing concrete, Sci. Rep. 9 (1) (2019) 1–12.

[52] T. Qureshi, A. Kanellopoulos, A. Al-Tabbaa, Encapsulation of expansive powder minerals within a concentric glass capsule system for self-healing concrete, Construct. Build. Mater. 121 (2016) 629–643.

[53] M. Kosarli, D. Bekas, K. Tsirka, A.S. Paipetis, Capsule-based self-healing polymers and composites, Self-Healing Polymer-Based Systems, 2020, pp. 259–278. Elsevier.

[54] J. Wang, H. Soens, W. Verstraete, N. De Belie, Self-healing concrete by use of microencapsulated bacterial spores, Cement Concr. Res. 56 (2014) 139–152.

[55] C.M. Dry, Design of self-growing, self-sensing, and self-repairing materials for engineering applications, Smart Materials, SPIE, 2001, pp. 23–29.

[56] V.C. Li, Y.M. Lim, Y.-W. Chan, Feasibility study of a passive smart self-healing cementitious composite, Compos. B Eng. 29 (6) (1998) 819–827.

[57] T. Nishiwaki, H. Mihashi, B.-K. Jang, K. Miura, Development of self-healing system for concrete with selective heating around crack, J. Adv. Concr. Technol. 4 (2) (2006) 267–275.

[58] T.D.P. Thao, T.J.S. Johnson, Q.S. Tong, P.S. Dai, Implementation of self-healing in concrete–proof of concept, IES J. Part A Civ. Struct. Eng. 2 (2) (2009) 116–125.

[59] X. Feng, N. Zhuo, H. Ningxu, D. Biqin, D.Z. Xuexiao, H. Ming Z, Self-healing mechanism of a novel cementitious composite using microcapsules, in: International Conference on Durability of Concrete Structures, Hangzhou, China, 2008.

[60] H. Mihashi, Y. Kaneko, T. Nishiwaki, K. Otsuka, Fundamental study on development of intelligent concrete characterized by self-healing capability for strength, Concr. Res. Technol. 11 (2) (2000) 21–28.

[61] G. Anglani, P. Antonaci, S.I.C. Gonzales, G. Paganelli, J.-M. Tulliani, 3D printed capsules for self-healing concrete applications, in: 10th International Conference on Fracture Mechanics of Concrete and Concrete Structures (FraMCoS-X), Bayonne, France, 2019.

[62] M. Araújo, S. Chatrabhuti, S. Gurdebeke, N. Alderete, K. Van Tittelboom, J.-M. Raquez, V. Cnudde, S. Van Vlierberghe, N. De Belie, E. Gruyaert, Poly (methyl methacrylate) capsules as an alternative to the ''proof-of-concept''glass capsules used in self-healing concrete, Cement Concr. Compos. 89 (2018) 260–271.

[63] C. Joseph, A.D. Jefferson, B. Isaacs, R. Lark, D. Gardner, Experimental investigation of adhesive-based self-healing of cementitious materials, Mag. Concr. Res. 62 (11) (2010) 831–843.

[64] K. Van Tittelboom, J. Wang, M. Araújo, D. Snoeck, E. Gruyaert, B. Debbaut, H. Derluyn, V. Cnudde, E. Tsangouri, D. Van Hemelrijck, N. De Belie, Comparison of different approaches for self-healing concrete in a large-scale lab test, Construct. Build. Mater. 107 (2016) 125–137.

[65] T.D.P. Thao, Quasi-Brittle self-healing materials: Numerical modelling and applications in civil engineering, National University of Singapore, Singapore, 2011.

[66] T.D.P. Thao, T.J.S. Johnson, Q.S. Tong, P.S. Dai, Implementation of self-healing in concrete – proof of concept, IES J. Part A Civ. Struct. Eng. 2 (2) (2009) 116–125.

[67] E. Gruyaert, K. Van Tittelboom, J. Sucaet, J. Anrijs, S. Van Vlierberghe, P. Dubruel, B.G. De Geest, J.P. Remon, N. De Belie, Capsules with Evolving Brittleness to Resist the Preparation of Self-Healing Concrete 66, 2016, 323.

[68] T.S. Qureshi, A. Kanellopoulos, A. Al-Tabbaa, Encapsulation of expansive powder minerals within a concentric glass capsule system for self-healing concrete, Construct. Build. Mater. 121 (2016) 629–643.

[69] V. Wiktor, H.M. Jonkers, Quantification of crack-healing in novel bacteria-based self-healing concrete, Cement Concr. Compos. 33 (7) (2011) 763–770.

[70] K. Sisomphon, O. Copuroglu, A. Fraaij, Application of encapsulated lightweight aggregate impregnated with sodium monofluorophosphate as a self-healing agent in blast furnace slag mortar, Heron 56 (1/2) (2011) 13–32.
[71] H. Liu, S. Qian, J. Van de Kuilen, W. Gard, M. de Rooij, E. Schlangen, W. Ursem, Self-healing of concrete cracks using hollow plant fibres, in: Proceedings of 2nd International Conference on Self Healing Materials, Chicago, IL, USA, 2009.
[72] M. Rauf, W. Khaliq, R.A. Khushnood, I. Ahmed, Comparative performance of different bacteria immobilized in natural fibers for self-healing in concrete, Construct. Build. Mater. 258 (2020), 119578.
[73] K. Van Tittelboom, N. De Belie, D. Van Loo, P. Jacobs, Self-healing efficiency of cementitious materials containing tubular capsules filled with healing agent, Cement Concr. Compos. 33 (4) (2011) 497–505.
[74] H. Mihashi, T. Nishiwaki, Y. Kaneko, N. Nishiyama, Development of smart concretes, in: 1st Fib Congress, Osaka, Japan, 2002.
[75] H. Huang, G. Ye, Application of sodium silicate solution as self-healing agent in cementitious materials, in: International Conference on Advances in Construction Materials through Science and Engineering, Hong Kong, China, 2011.
[76] I. Kaltzakorta, E. Erkizia, Silica microcapsules encapsulating epoxy compounds for self-healing cementitious materials, in: 3rd International Conference on Self Healing Materials, Bath, UK, 2011.
[77] Z. Yang, J. Hollar, X. He, X. Shi, A self-healing cementitious composite using oil core/silica gel shell microcapsules, Cement Concr. Compos. 33 (4) (2011) 506–512.
[78] H. Xia, Self-healing of engineered cementitious composites (ECC) in concrete repair system, Delft University of Technology, Delft, The Netherlands, 2010.
[79] D. Janssen, Water encapsulation to initiate self-healing in cementitious materials, Delft University of Technology, Delft, The Netherlands, 2011.
[80] J.Y. Wang, N. De Belie, W. Verstraete, Diatomaceous earth as a protective vehicle for bacteria applied for self-healing concrete, J. Ind. Microbiol. Biotechnol. 39 (4) (2012) 567–577.
[81] S. Sangadji, E. Schlangen, Self healing of concrete structures - novel approach using porous network concrete, J. Adv. Concr. Technol. 10 (5) (2012) 185–194.
[82] X. Zhang, C. Qian, A new type capsule-based healing agent for concrete and its protective function of spores, Smart Mater. Struct. 29 (10) (2020), 105035.
[83] B. Saleem, A. Hussain, A. Khattak, A. Khan, Performance evaluation of bacterial self-healing rigid pavement by incorporating recycled brick aggregate, Cement Concr. Compos. 117 (2021), 103914.
[84] L. Jiang, G. Jia, C. Jiang, Z. Li, Sugar-coated expanded perlite as a bacterial carrier for crack-healing concrete applications, Construct. Build. Mater. 232 (2020), 117222.
[85] M. Wu, X. Hu, Q. Zhang, W. Cheng, D. Xue, Y. Zhao, Application of bacterial spores coated by a green inorganic cementitious material for the self-healing of concrete cracks, Cement Concr. Compos. 113 (2020), 103718.
[86] L.S. Ebers, A. Arya, C. Bowland, W. Glasser, S. Chmely, A. Naskar, M.P. Laborie, 3D printing of lignin: challenges, opportunities and roads onward, Biopolymers (2021), e23431.
[87] D. Bajwa, G. Pourhashem, A.H. Ullah, S. Bajwa, A concise review of current lignin production, applications, products and their environmental impact, Ind. Crop. Prod. 139 (2019), 111526.
[88] B. Lothenbach, Thermodynamic equilibrium calculations in cementitious systems, Mater. Struct. 43 (10) (2010) 1413–1433.
[89] Z. Lv, H. Chen, Analytical models for determining the dosage of capsules embedded in self-healing materials, Comput. Mater. Sci. 68 (2013) 81–89.
[90] A. C192, ASTM C192/C192M—16a standard practice for making and curing concrete test specimens in the laboratory, ASTM Standard Book, 2020, pp. 4–9.
[91] A. C143, ASTM-C143/C143M-20Standard Test Method for Slump of Hydraulic-Cement Concrete, ASTM International, West Conshohocken, PA, 2020.
[92] A. C39, ASTM-C39/C39M-20 Standard Test Method for Compressive Strength of Cylindrical Concrete Specimens, ASTM International, West Conshohocken, PA, West Conshohocken, 2020.
[93] A. C109, ASTM C109/C109M-20b Standard Test Method for Compressive Strength of Hydraulic Cement Mortars (Using 2-in. or [50 mm] Cube Specimens), 2020. West Conshohocken, PA.
[94] A. C496, ASTM-C496/C496M-17 Standard Test Method for Splitting Tensile Strength of Cylindrical Concrete Specimens, ASTM International, West Conshohocken, PA, 2017.
[95] L. Tognotti, A. Malotti, L. Petarca, S. Zanelli, Measurement of ignition temperature of coal particles using a thermogravimetric technique, Combust. Sci. Technol. 44 (1–2) (1985) 15–28.
[96] A. C1876, ASTM C1876-19 Standard Test Method for Bulk Electrical Resistivity or Bulk Conductivity of Concrete, ASTM International, West Conshohocken, PA, 2019.
[97] E. Melro, A. Filipe, D. Sousa, A.J. Valente, A. Romano, F.E. Antunes, B. Medronho, Dissolution of kraft lignin in alkaline solutions, Int. J. Biol. Macromol. 148 (2020) 688–695.
[98] H. Huang, G. Ye, Numerical studies of the effects of water capsules on self-healing efficiency and mechanical properties in cementitious materials, Adv. Mater. Sci. Eng. (2016) 2016.
[99] D. Jung, Performance and properties of embedded microspheres for self-repairing applications, Citeseer, 1997.
[100] J. Wei, C. Meyer, Degradation mechanisms of natural fiber in the matrix of cement composites, Cement Concr. Res. 73 (2015) 1–16.
[101] J. Wei, Degradation behavior and kinetics of sisal fiber in pore solutions of sustainable cementitious composite containing metakaolin, Polym. Degrad. Stabil. 150 (2018) 1–12.
[102] J. Zakzeski, P.C. Bruijnincx, A.L. Jongerius, B.M. Weckhuysen, The catalytic valorization of lignin for the production of renewable chemicals, Chem. Rev. 110 (6) (2010) 3552–3599.